

# Water Resources Research®

## RESEARCH ARTICLE

10.1029/2021WR031013

### Key Points:

- Paired catchment method is modified for the use of detecting changes in catchment water balance, including water storage change
- The decreased evapotranspiration and the increased streamflow due to the 2009 Victorian Bushfires are temporally asynchronous
- The water storage increase in a wetter climate may be less than expected for burned catchments

### Supporting Information:

Supporting Information may be found in the online version of this article.

### Correspondence to:

Y. Zhang,  
zhangyq@igsnrr.ac.cn

### Citation:

Xu, Z., Zhang, Y., Zhang, X., Ma, N., Tian, J., Kong, D., & Post, D. (2022). Bushfire-induced water balance changes detected by a modified paired catchment method. *Water Resources Research*, 58, e2021WR031013. <https://doi.org/10.1029/2021WR031013>

Received 7 AUG 2021

Accepted 7 OCT 2022

### Author Contributions:

**Conceptualization:** Zhenwu Xu, Yongqiang Zhang

**Data curation:** Zhenwu Xu

**Formal analysis:** Zhenwu Xu

**Funding acquisition:** Yongqiang Zhang

**Investigation:** Zhenwu Xu

**Methodology:** Zhenwu Xu, Yongqiang Zhang

**Project Administration:** Yongqiang Zhang

**Resources:** Yongqiang Zhang

**Software:** Zhenwu Xu

**Supervision:** Yongqiang Zhang

**Validation:** Zhenwu Xu

**Visualization:** Zhenwu Xu

**Writing – original draft:** Zhenwu Xu

**Writing – review & editing:** Zhenwu Xu, Yongqiang Zhang, Xuanze Zhang, Ning Ma, Jing Tian, Dongdong Kong, David Post

## Bushfire-Induced Water Balance Changes Detected by a Modified Paired Catchment Method

Zhenwu Xu<sup>1,2</sup> , Yongqiang Zhang<sup>1</sup> , Xuanze Zhang<sup>1</sup>, Ning Ma<sup>1</sup> , Jing Tian<sup>1</sup>, Dongdong Kong<sup>3</sup> , and David Post<sup>4</sup> 

<sup>1</sup>Key Laboratory of Water Cycle and Related Land Surface Processes, Institute of Geographic Sciences and Natural Resources Research, Chinese Academy of Sciences, Beijing, China, <sup>2</sup>University of Chinese Academy of Sciences, Beijing, China,

<sup>3</sup>Department of Atmospheric Science, School of Environmental Studies, China University of Geosciences, Wuhan, China,

<sup>4</sup>CSIRO Land and Water, Black Mountain, Canberra, ACT, Australia

**Abstract** While bushfires are often regarded as a vital trigger that alters the partitioning of hydrological fluxes, their role in water balance changes remains poorly quantified, especially in regions where the impacts of frequent bushfires and climate variability overlap. Here, we estimated the fire-induced water balance changes based on a modified paired catchment method that considers the partial effect of annual precipitation differences. In the application for eight forested catchments impacted by the 2009 Victorian Bushfires with multiple burned areas (12%–89%), we found that evapotranspiration declined by  $33 \pm 20 \text{ mm yr}^{-1}$  (mean  $\pm$  standard deviation) and streamflow increased by  $68 \pm 32 \text{ mm yr}^{-1}$  during the post-fire decade. For the interannual changes within this decade, the decline in evapotranspiration due to fires gradually recovered after the first year since bushfires, while the increase in streamflow mostly peaked in the second or third year and diminished in subsequent years. We surmised that such asynchronous responses of the two fluxes to bushfires occurred with the initial increase and the later decrease in terrestrial water storage. Averaged for the post-fire decade, there seems to be an overall decline in terrestrial water storage for burned catchments relative to unburned catchments.

**Plain Language Summary** Apart from high temperature and burning biomass, bushfires can induce dramatic changes in plant water use and water yield in catchments during post-fire years. Its impact on water resources is often compounded with climate change. In early 2009, large forest fires swept many parts of Victoria, Australia. Using a set of burned and unburned catchments and high-resolution water balance data, we found that bushfires caused asynchronous decreases in evapotranspiration and increases in streamflow. The different magnitudes of the changes in the two fluxes may indicate a decline in terrestrial water storage for burned catchments when compared with that of unburned catchments. These findings advance our understanding of the role of bushfires on hydrological fluxes and terrestrial water storage in a changing climate.

## 1. Introduction

Forests influence climate through physical, chemical, and biological processes and provide ecological and social services to natural systems and humankind, including the protection of water resources (Bladon et al., 2014; Bonan, 2008; Meier et al., 2021; Zeng et al., 2021). In southeast Australia, forests are prone to be disturbed by bushfires (also known as fires, or wildfires), which cause abrupt changes by biomass burning and bring long-lasting changes in vegetation structure and composition (Boer et al., 2020; Keeley et al., 2019). Subsequently, the change of vegetation cover alters regional hydrological processes during the post-fire period that are marked by vegetation recovery and forest regeneration. Such ecological and hydrological responses to bushfires are more likely to happen with anthropogenic climate change (Brey et al., 2021; Fang et al., 2021) and the changes may be irreversible. Thus recent concerns of potential increases in global and regional forest fire activities also highlight the hydrological consequences of bushfires, as there is evidence that increased runoff and erosion from burned areas disrupted water supplies (Abram et al., 2021; Canadell et al., 2021; Hallema, Robinne, & Bladon, 2018; Holden et al., 2018; McWethy et al., 2019; Robinne et al., 2021).

A wealth of literature based on field measurements and model experiments in southeast Australia has unraveled the dramatic changes in the partitioning of water use and water yields after bushfires (Kuczera, 1987; Kumar et al., 2021; Lane et al., 2006; Langford, 1976). Similar to burned forests elsewhere, the removal of vegetation

cover would directly reduce evapotranspiration (ET) by changing its partitioning, including reduced rainfall interception and transpiration, which exceed the increased soil evaporation due to more available energy for evaporation. Its recovery trajectory can be related to the change of stand structure, for example, leaf area index (LAI) and sapwood area (Nolan, Lane, et al., 2014; Nolan et al., 2015). The initial increase in streamflow ( $Q$ ) after severe forest fires is mainly attributed to the vegetation removal that reduces evapotranspiration (Feikema et al., 2013; Nolan et al., 2015; Watson et al., 2001), and the changed soil hydraulic properties (e.g., the enhanced soil water repellency) that induce accentuated runoff and peak flows (Noske et al., 2016; Nyman et al., 2011; Sheridan et al., 2007; Van Der Sant et al., 2018). In other forested catchments around the globe, initial increases in streamflow are also very common (Blount et al., 2019; Maina & Siirila-Woodburn, 2020; Mayor et al., 2007; Seibert et al., 2010; Stoof et al., 2012). However, the distinctness of bushfire impacts on hydrological processes in southeast Australia lies in the forest composition (mostly dominated by different species of eucalyptus) and the different tree recovery trajectory that controls the ET changes (recover via seedlings vs. recover via resprouting) (Nolan, Lane, et al., 2014; Nolan et al., 2015; Vertessy et al., 2001). For example, apart from the similar initial increases in water yields compared with global burned forests (Heath et al., 2015; Larsen et al., 2009; Letey, 2001), the long-term water yields are projected with ongoing reduction for ~150 years in the regrowth “ash” forests, which recover via seedlings and require a higher water use than mature forests (Brookhouse et al., 2013; Kuczera, 1987; Vertessy et al., 2001). In comparison, the mixed species eucalypt forests, which are more common in southeast Australia and recover via resprouting, require less time for full recovery (10–12 years) (Nolan et al., 2015). Overall, it is expected that the fire impacts are highly variable across regions and time scales (Maina & Siirila-Woodburn, 2020; Wine, Makhnin, & Cadol, 2018) and are a syndrome of burned severity and vegetation recovery metrics (Nolan, Lane, et al., 2014; Nolan et al., 2015), precipitation (Feikema et al., 2013; Lane et al., 2010), aridity and initial soil water content (Feikema et al., 2013; Noske et al., 2016; Van Der Sant et al., 2018), and prior disturbance legacy impacts (Bowd et al., 2021). The complex nature of vegetation changes and the hydrological responses after bushfires make it rather difficult to precisely quantify the role of fires at the catchment and the regional scale.

By influencing vegetation and soil properties, bushfire alters the partitioning of hydrological fluxes (Blount et al., 2019; Kumar et al., 2021; Montes-Helu et al., 2009), and its impact was compounded with climate change (Feikema et al., 2013; Guo et al., 2021; Zhou et al., 2015). Longer droughts (Cardil et al., 2019; Littell et al., 2016; Turco et al., 2017) and higher climate variabilities (Brey et al., 2021; Fang et al., 2021; Swain, 2021) make fires more prone to happen and the post-fire impact more variable. As fires usually happen during droughts, the initial increases in runoff due to reduced canopy may not occur or be detected because of the soil water deficit (Feikema et al., 2013). In contrast, when the climate is shifted to a wet scenario, the increase in runoff and erosion in most severe burnt and water-repellent soils can be phenomenal when there is intensive rainfall after fires, which may evolve as debris flows and flash floods (Kean et al., 2012; Liu et al., 2022; Nasseri, 1989; Versini et al., 2012). These differences in runoff production indicate even though fires have changed vegetation cover and soil to varying degrees, the timing and the magnitude of their hydrological impact can be dependent on the climate (Maina & Siirila-Woodburn, 2020). Therefore, disentangling the relative contributions of bushfires and climate in the hydrological changes is important for understanding the role of fires on the hydrological processes in a changing climate.

As the bushfire impact on the hydrological partitioning of ET and  $Q$  is highly variable under climate variability, it is more difficult to estimate the concurrent change of terrestrial water storage ( $\Delta S$ ) which is essential for explaining the changes in water balance. The storage-discharge dynamics are not stationary under vegetation changes (Bart & Tague, 2017; Cheng et al., 2017). The higher discharge of streams and rivers is usually attributed to decreased canopy interception and evapotranspiration caused by vegetation removal, leaving more soil water for runoff production (Blount et al., 2019; Boisrame et al., 2019; Stoof et al., 2012). However, the changed soil hydrologic properties, for example, soil water repellency effects on infiltration, are also found to mostly increase overland flow and peak flow after fires (Ebel et al., 2012; Nyman et al., 2014; Shakesby & Doerr, 2006). These two different paths naturally have different impacts on the soil water and groundwater budget at the hillslope scale (Atchley et al., 2018) and the catchment-scale result can be more intricate (Bart & Tague, 2017). Although the Gravity Recovery and Climate Experiment (GRACE) satellite observations have substantially facilitated the detection of fire-induced water storage loss for large-scale studies (e.g., Han et al., 2017), the inherent low resolution of GRACE satellite signals ( $3^\circ$ ) prevents the explicit representation of the water storage change for small to medium headwaters, typically at the order of  $<500 \text{ km}^2$ . Therefore, the quantification of the change of catchment-scale

$\Delta S$  in these headwater catchments will inevitably rely on the water balance principle and the other three water balance components. However, such quantification is challenging as it requires both high-resolution data and a reliable method for separating the fire impacts.

Hydrological changes after disturbances can be extracted from the impact of climate variability by a set of approaches, including statistical changing point analysis (Hallema, Sun, et al., 2018), observation-modeling comparison (Van Loon & Van Lanen, 2013), upstream-downstream comparison (Rangecroft et al., 2019), pre-post-disturbances comparison (Liu et al., 2016), large-scale screening (Gupta et al., 2014) and paired catchment method (PCM). However, all methods have limitations in their use, such as the possible system bias in observation-modeling comparison and the requirement of large data for large-scale screening. Among them, PCM is often recognized as the most simple and robust method for detecting the effects of disturbances on catchment-scale hydrology (Bart & Hope, 2010; Brown et al., 2005; Cheng et al., 2017; Sun, Song, et al., 2020; Van Loon et al., 2019; Zhao et al., 2012), though it requires a good setup of paired catchments. Fire impacts are separated by comparing the water yields of a burned catchment with that of an unburned donor catchment, which has a similar climate, forest cover, soil, and hydrological fluxes (Bart & Hope, 2010). However, its potential is not fully explored yet for a joint comparison of all water balance components, especially for the water storage change. Almost no paired catchment studies have included the changes in water storage due to the limited approaches in getting reliable water storage data in small headwaters (McDonnell et al., 2018). Meanwhile, it is rare to use the PCM for median-sized catchments as a concern of the difficulty in keeping the hydrological similarity as their size and distance increase. Even so, it is still worthwhile to explore if the state-of-the-art water balance data from observations and remote sensing can be used for quantifying the water balance changes with the data-based PCM analysis.

In this paper, we investigate the bushfire impact on the water balance changes in eight forested headwater catchments, with special concerns on the possible changes in post-fire terrestrial water storage. The 2009 Victorian Bushfires, which occurred at the end of the Millennium Drought (~1997–2009, southeast Australia) and followed by strong La Niña conditions that brought very high precipitation (2010–2011), provide a natural experiment for understanding how catchment water balance responds to bushfires when climate condition shifts (see details in Section 2.1). The PCM was extended to be used for medium-sized basins (~100–500 km<sup>2</sup>) and was modified to quantify the post-fire changes in catchment water balance with a set of burned and unburned catchments. The major objective of this study is to develop a robust PCM method for (a) unraveling the temporal dynamics of fire-induced changes in hydrological flux partitioning of ET and  $Q$ , (b) estimating the possible fire impact on the terrestrial water storage based on the water balance principle, and (c) comparing the role of bushfires and climate variability in controlling the total changes of hydrological fluxes.

## 2. Data and Methods

### 2.1. The 2009 Victorian Bushfires

Eastern Australia's temperate broadleaf forests, dominated by eucalypts, are among the most fire-prone ecosystems in the world, and major fires are relatively common (Boer et al., 2020; Langford, 1976). Among those mega-fires, the 2009 Victorian Bushfires, better known as the Black Saturday Bushfires, were a conglomerate of over 300 grass, scrub, or forest fires extending over much of Victoria during early February (summer in Australia), with major influences on the evergreen broadleaf forests (EBF) located on the east of Melbourne (Figure 1). The bushfires occurred with heatwaves on 7 February 2009, the hottest day ever recorded in the state of Victoria, Australia, with air temperatures reaching at 46.4°C (Bureau of Meteorology, 2010).

The 2009 Victorian Bushfires occurred at the end of the “Millennium Drought” (~1996–2009, Peterson et al., 2021; Van Dijk et al., 2013), the worst drought on record for southeast Australia with the longest uninterrupted series of years with below-median rainfall since at least 1900. Prevailing El Niño events explained about two-thirds of the rainfall deficit in eastern Australia. Following the drought and the fires, 2010/2011 was marked by strong La Niña conditions that brought very high precipitation and large-scale flooding to many parts of southeast Australia (Ummenhofer et al., 2015). Compound influences of the shifted climate condition and large forest fires are expected to contribute to the change of hydrological fluxes in burned areas.

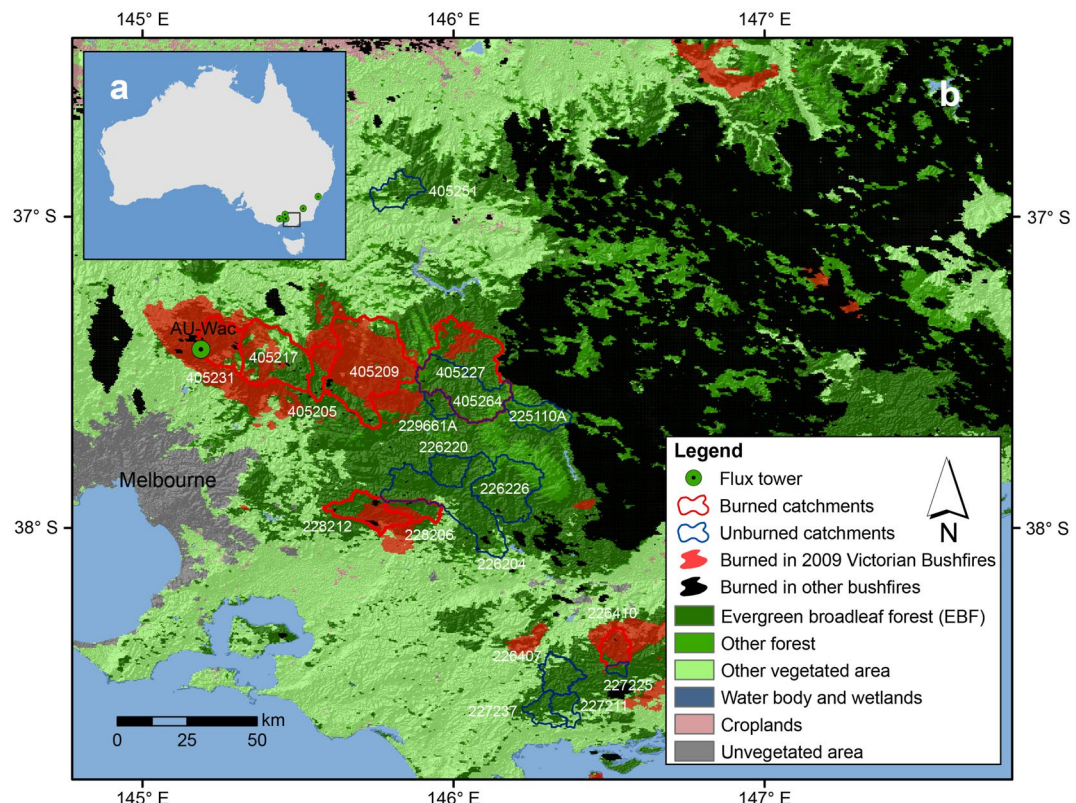


**Figure 1.** (a) The geographical location of the study area and (b) the unregulated burned catchments impacted by the 2009 Victorian Bushfires and unimpacted unburned catchments. The burned areas account for 12%–89% of the total areas of burned catchments (56% on average), with the most severe burning occurring in catchment #405231 (89%). Catchment #405264 is the upstream catchment and a part of catchment #405227, which received the most minor burning (12%). Note that not all unburned catchments were used as donor catchments, as presented in Table 2. In panel (a), observed evapotranspiration data from the five flux tower sites (including the one displayed in panel (b), AU-Wac) were used for calibrating the Penman-Monteith-Leuning Version 2 model.

## 2.2. Data

The climate data during 1982–2018 were obtained from the SILO Data Drill that was produced by the Queensland Department of Environment and Resource Management (Jeffrey et al., 2001). The daily climate variables, including precipitation ( $P$ ), incoming solar radiation, vapor pressure, minimum temperature, and maximum temperature, have a  $0.05^{\circ}$  ( $\sim 5 \text{ km}$ ) spatial resolution.

The streamflow data were obtained mostly from Hydrologic Reference Stations (HRS), which are well-maintained river gauges of records available from the Australian Bureau of Meteorology. With strict selection guidelines, these catchments are mostly unregulated with minimal land use change. Overall, data from these stations have a low level of missing and can be used to estimate trends in long-term and seasonal water availability from climate variability and change. Considering the demand for continuous data for the paired catchment study, data from 1982 to 2018 was used. Furthermore, we used the GR4J hydrological model (modèle du Génie Rural à 4 paramètres Journalier) (Perrin et al., 2003) to interpolate the streamflow data when the missing portion is less than 10%, which has little impact on the estimation of annual streamflow and its trends (Zhang & Post, 2018).

All remote sensing products were obtained from the Google Earth Engine (GEE), which provides Moderate Resolution Imaging Spectroradiometer (MODIS) Collection (C) 6 products from 2001 to 2018. The burned area data were the C6 MCD64A1 product (Giglio et al., 2018), which has a 500-m spatial resolution and manages a lower temporal uncertainty compared to the C5.1 MCD64A1 and MCD45A1 products. Albedo was obtained from the C6 MCD43A3 product (Schaaf & Wang, 2015). The LAI data were obtained from the C6 MOD15A2H product (Myneni et al., 2015) and were smoothed by the weighted Whittaker smoother (wWHd) (Kong et al., 2019). Although early research pointed out the overestimation of LAI in the MODIS C4 product in some Australian open

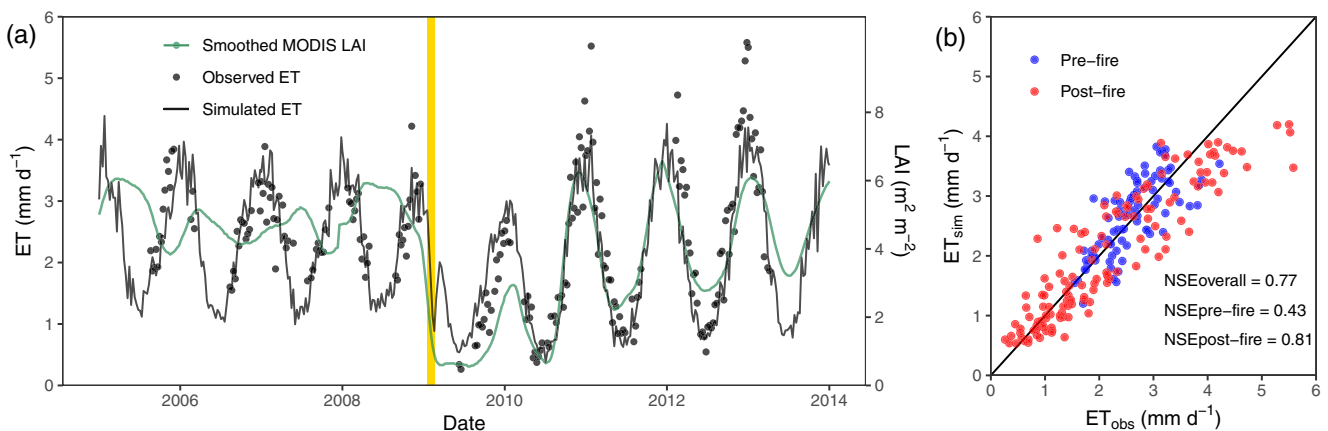


**Figure 2.** (a) Time series of the observed evapotranspiration (ET) in flux site AU-Wac and the Penman-Monteith-Leuning Version 2 model simulated ET, and (b) their scatterplot. The yellow line denotes the timing of the 2009 Victorian Bushfires.

forests and woodlands (Hill et al., 2006), the overestimation was documented to be improved since the MODIS C5 product (Sea et al., 2011). In this study, the smoothed MODIS C6 LAI data seem to be able to characterize the dramatic decreases of LAI during the fire event and the following long-term recovery at site and catchment scales (Figure 2 and Figure S1 in Supporting Information S1). Meanwhile, it can capture the basic vegetation dynamics before and after fires by a visual confirmation with the Landsat 7 images (Figure S2 in Supporting Information S1). Albedo also significantly decreased during the fires (Figure S1 in Supporting Information S1), which may be attributed to the darkening effect of abundant precipitation (Saha et al., 2017).

A three-layer diagnostic model, that is, the Penman-Monteith-Leuning Version 2 (PML-V2) model, was used for modeling evapotranspiration (ET) (Zhang et al., 2019). The PML-V2 model was based on the classical Penman-Monteith (PM) equation (Monteith, 1965). With a series of improvements, the PML-V2 model can estimate the three ET components of soil evaporation ( $E_s$ ), transpiration ( $E_c$ ), and evaporation of precipitation intercepted by vegetation ( $E_i$ ) more accurately. Based on the LAI, the total available energy is partitioned into the canopy absorption and the soil absorption to estimate  $E_c$  and  $E_s$  (Leuning et al., 2008). PML-V2 also uses a widely adopted rainfall interception model of Gash to estimate  $E_i$  (Zhang et al., 2016). In comparison with other PM-based models (e.g., MODIS MOD16A2, Mu et al., 2011), the most important features of PML-V2 are (a) deriving canopy conductance ( $G_c$ ) from the photosynthesis with the constraint of vapor pressure deficit as the transpiration and the photosynthesis are fully coupled, and (b) considering the impact of CO<sub>2</sub> concentration on carbon assimilation and  $G_c$  (Ma & Zhang, 2022; Zhang et al., 2019). Therefore, it can simulate the changes of ET components in response to the post-fire reductions and recovery of LAI and surface albedo, including the decreased interception and transpiration of trees, and the increased soil evaporation (Figure S3 in Supporting Information S1).

In addition, we ran the PML-V2 model using the local climate forcing that is available in the SILO Data Drill. For other forcing inputs, we kept using the data that were originally used in producing the global PML-V2 ET data set, including the Global Land Data Assimilation System V2.1 (GLDAS 2.1) (Beaudoing & Rodell, 2020) climate forcing (longwave radiation, wind speed, air pressure) and the global monthly atmospheric CO<sub>2</sub> concentration data from National Oceanic and Atmospheric Administration (NOAA). All the climate forcing was aggregated into the same spatial-temporal resolution of MODIS inputs, that is, 8-day temporal resolution and 500-m spatial resolution.

The measured latent heat flux data (LE) from five local EBF flux sites (AU-Wac, AU-Tum, Au-Cum, AU-Whr, AU-Wom, Figure 1a) were used for constraining ET modeling for EBF in southeast Australia. In particular, the AU-Wac flux tower was destroyed by the 2009 Victorian Bushfires and rebuilt after the fires (Figure 1b), covering approximately 3-year pre-fire and 3-year post-fire LE estimates. According to the 500-m resolution MODIS grid cell that covers the AU-Wac tower, MODIS LAI dramatically dropped by 88% during the fires. It remained noticeably low for the first year, indicating a strong post-fire footprint on vegetation and ET. Data from these flux sites were collected by the OzFlux project (Beringer et al., 2016), which is a part of the global flux project

FLUXNET2015 (Pastorello et al., 2020), providing high-quality daily fluxes that were processed by a strict gap-filling method from the original 30-min data. However, this data set did not cover the post-fire observations of the AU-Wac, which were instead obtained from OzFlux. The original 30-min LE data were censored with data quality and then gap-filled using REddyProc (Wutzler et al., 2018), the same program used for producing the FLUXNET2015 database. To aggregate these data to 8-day resolution, we only used full coverage of high-quality daily data (with at least half coverage of measured and high-quality gap-filled data, quality control QC > 0.5) to be averaged as 8-day observed ET data for parameterizing PML-V2 modeling (Ma et al., 2021).

Since this study aims to provide a comparative separation of the impact of bushfires and climate variability, we assumed that these two factors are both important in our analysis: (a) ET responses to fires (represented by data from the fire-impacted AU-Wac flux site) and (b) ET variations under climate variability (represented by data from all five flux sites). Therefore, we calibrated the PML-V2 model with the following objective function ( $F$ ) to maximize both Nash-Sutcliffe Efficient (NSE).

$$F = 2 - \text{NSE}_{\text{AU-Wac}} - \text{NSE}_{\text{all}} \quad (1)$$

$$\text{NSE} = 1 - \frac{\sum_{i=1}^n |\text{ET}_{\text{sim},i} - \text{ET}_{\text{obs},i}|^2}{\sum_{i=1}^n |\text{ET}_{\text{obs},i} - \overline{\text{ET}}_{\text{obs}}|^2} \quad (2)$$

where  $\text{ET}_{\text{sim},i}$  and  $\text{ET}_{\text{obs},i}$  are the simulated and observed 8-day ET in the  $i$ th record, respectively.  $\overline{\text{ET}}_{\text{obs}}$  is mean observed ET.

In calibration mode, the overall NSE reaches 0.77 for AU-Wac ET observations which cover both pre-fire and post-fire records (Figure 2). The ET variation in the post-fire period is also well simulated (NSE = 0.81). The only exception is that some observed high ET extremes ( $\text{ET} > 4.5 \text{ mm d}^{-1}$ ) cannot be captured by the model for the burned flux site AU-Wac. However, we found that they are not biases exclusively attributed to the model's ability in estimating ET after bushfires, as similar phenomena also exist in summers during 2009–2014 for the unburned flux sites AU-Tum and AU-Wom (Figure S4 in Supporting Information S1). For all sites, the NSE is 0.77 and 0.76 in the calibration and the leave-one-out cross-validation modes, respectively (Figure S5 in Supporting Information S1). Especially, the NSE is 0.72 for simulating ET in the burned AU-Wac site in the cross-validation mode using the calibrated parameters from the other four unburned sites. There is only little degradation in model performance from the calibration mode to the leave-one-out cross-validation mode, indicating the robustness of the model and the calibrated parameters. The above testing shows that the PML-V2 is reliable for characterizing ET variations in these burned and unburned EBFs (Figure S4 in Supporting Information S1).

To increase the robustness of our results, we also used other two high-resolution ET data sets: a widely used global 8-day ET product (MODIS MOD16A2, 500-m) (Mu et al., 2011; Running et al., 2017) and a local monthly ET product for Australia (CSIRO MODIS Reflectance-based Scaling EvapoTranspiration, CMRSET, 30-m) (Guerschman et al., 2022). Compared with them, the PML-V2 model yields better ET estimates for the burned EBF flux site AU-Wac (NSE increased by 0.22 and 0.20, Figure S6 in Supporting Information S1), and similarly better ET estimates across the other four unburned EBF flux sites (Figure S7 in Supporting Information S1). Therefore, we mainly used the ET estimates from PML-V2 to analyze the results. In Section 4.1, we used all three ET products to quantify the uncertainty of estimating fire-induced ET and water storage change due to the selection of ET data.

Based on the water balance principle, catchment-scale annual water storage change ( $\Delta S$ ) can be derived from other three components: annual precipitation ( $P$ ), ET, and streamflow ( $Q$ ).

$$\Delta S = P - \text{ET} - Q \quad (3)$$

Since  $P$ , ET and  $Q$  are from three independent measured or simulated hydrological fluxes,  $\Delta S$  can be noticeably biased in its mean value (Figure S8 in Supporting Information S1). However, the variability of  $\Delta S$  is kept while removing mean from pre-fire averages for each catchment ( $\Delta S$  anomaly). The GRACE data is a reference of  $\Delta S$  at the regional scale, which can be computed by the differences in the terrestrial water storage anomaly data (TWSA) between consecutive Decembers (Ma et al., 2021; Nie et al., 2015). In comparison with the observed regional GRACE  $\Delta S$  data (here using GRACE JPL RL06 mascon product, Watkins et al., 2015; Wiese et al., 2016; Wiese et al., 2018), we found that the ensemble water-balance-derived  $\Delta S$  anomaly has a similar variation ( $R^2 = 0.73$  for

**Table 1**  
*Summary of Catchment Characteristics*

ID	Station name	Area (km <sup>2</sup> )	Averaged elevation (m)	MAP <sup>a</sup> (mm yr <sup>-1</sup> )	MAQ <sup>a</sup> (mm yr <sup>-1</sup> )	MAT <sup>a</sup> (°C)	p <sub>EBF</sub> <sup>b</sup> (%)	BFI <sup>c</sup>	Burned area (%)
405231	Flowerdale	179	550	920	78	12.4	87 ± 2	0.73	89
226410	Koornalla	86	416	1,040	173	12.5	96 ± 2	0.45	86
405209	Taggerty	629	630	1,011	282	12.1	78 ± 1	0.77	75
228212	Tonimbuk	169	306	1,233	118	13.0	96	0.71	55
405205	Murrindindi above Colwells	106	702	1,037	306	11.8	100	0.80	53
405217	Devlins Bridge	361	461	857	110	12.9	65 ± 1	0.67	43
228206	Neerim	85	448	1,158	146	12.5	94 ± 2	0.76	36
405227	Jamieson	627	790	1,050	289	11.4	83	0.77	12
225110A	D/S Johnsons Creek	132	865	1,172	229	10.8	60	0.66	/
226204	Willow Grove	558	485	1,114	185	12.4	89	0.79	/
226220	Noojee	102	576	1,164	180	12.0	99	0.77	/
226226	Tanjil Junction	299	654	1,174	317	11.5	78	0.77	/
227211	Toora	65	315	1,004	274	13.2	68	0.48	/
227225	Fischers	21	492	1,199	258	12.3	100	0.70	/
227237	Toora	75	273	1,000	237	13.3	72	0.46	/
229661A	RD 1	55	738	1,062	186	11.7	98	0.80	/
405251	Ancona	122	563	688	46	12.8	59	0.57	/
405264	D/S of Frenchman Creek Junction	335	863	1,095	338	10.9	76	0.72	/
226407	Boolarra	116	337	1,049	207	13.0	87	0.62	/

<sup>a</sup>Multiyear (2001–2008) mean annual precipitation, streamflow, air temperature. <sup>b</sup>The areal coverage of evergreen broadleaf forest, the “±” denotes the standard deviation of evergreen broadleaf forest summarized by annual land cover in the study period. <sup>c</sup>Baseflow index, that is, the portion of averaged baseflow on averaged streamflow.

burned catchments,  $R^2 = 0.70$  for all catchments) with the GRACE observed  $\Delta S$  value in 2004–2016 (Figure S9 in Supporting Information S1). As the GRACE data was produced initially from a 3° satellite signal, their similarity indicates that the water-balance-derived  $\Delta S$  anomaly can roughly capture the variability of water storage changes at the regional scale, though the manner of variations seems to diverge between the burned catchments and all catchments during some post-fire years (Figure S9 in Supporting Information S1).

Due to the limit of the MODIS product, the modeled ET and the water-balance-derived  $\Delta S$  are available for 2001–2018. The  $P$  and  $Q$  are available for 1982–2018. While using the modified PCM, 27 years (1982–2008) of  $Q$  and 8 years (2001–2008) of ET are available for calibration. Ten years (2009–2018) of all water balance data are available for evaluating the fire impact after the 2009 Victorian Bushfires.

### 2.3. Catchments

A specific criterion was performed to examine the similarity of catchments in climate, vegetation cover, and hydrologic conditions. After having good quality control of streamflow data (missing portion <10% and the missing data are gap-filled using GR4J, detailed information see Method S1, Figures S10 and S11 in Supporting Information S1) and focusing our study on forest fires in EBF (areal coverage of EBF,  $p_{EBF} > 65\%$ , Table 1), we obtained 19 unregulated forested catchments located near the 2009 Victorian Bushfires (Table 1), most of which are included in the HRS list (16 of them). Then we divided them into burned and unburned catchments. To eliminate the possible overlapping impacts of multiple fires, the burned catchments are assumed to be the catchments that were mainly burned in the 2009 Victorian Bushfires (the coverage of the burned area is larger than 10% in the 2009 Victorian Bushfires and the burned area is less than 10% in the sum of other fires). According to the MCD64A1 burned area product, the burned area of the eight selected catchments ranges from 12% to 89% (56%

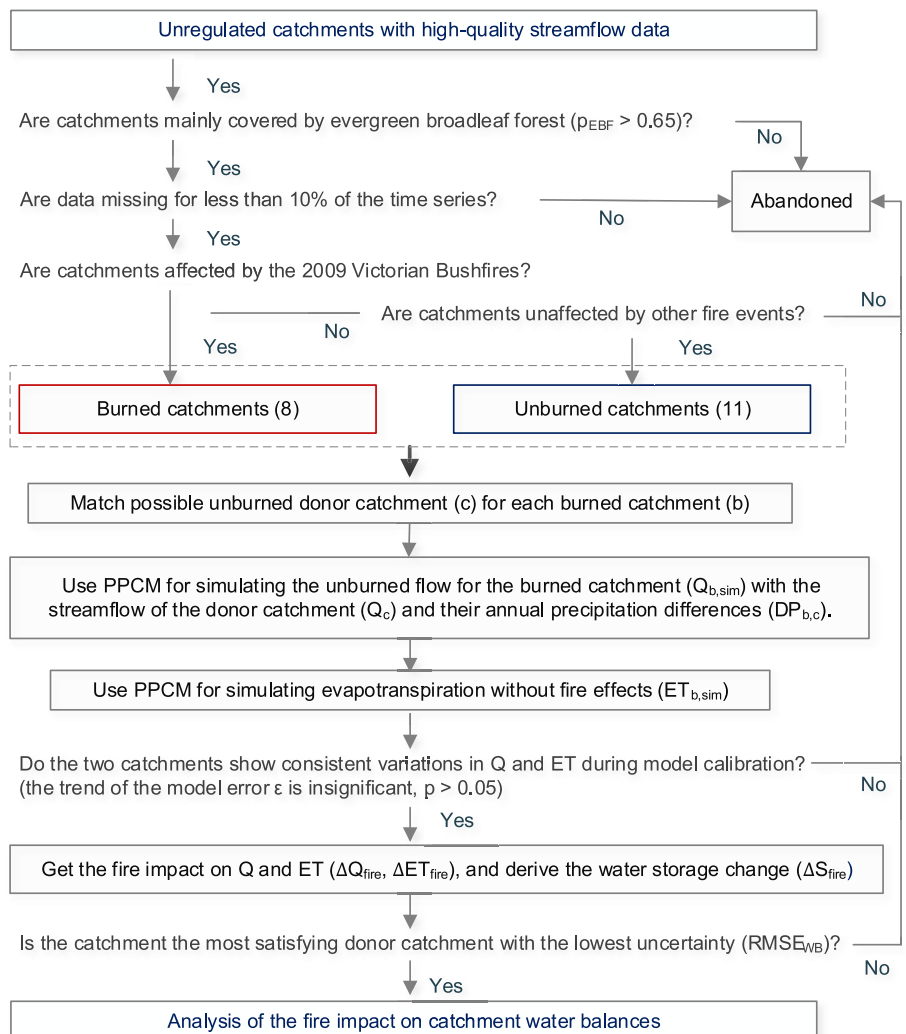


**Figure 3.** Flowchart of selecting suitable paired catchments to analyze the bushfire impact.

on average, Table 1). In comparison, the 11 possible unburned donor catchments are assumed to receive little or no impact from bushfires (the burned area is less than 10% of the sum of all fires).

Since there are no uniform and quantifiable criteria for the requirements of a donor catchment (Brown et al., 2005; Van Loon et al., 2019), we tried to use any unburned catchment as a possible donor catchment to represent an unburned state of the burned catchment. The hydrological similarity is evaluated based on pre-fire data to get the optimal donor catchment for each catchment (Figure 3). The bushfire impact on hydrological fluxes is then separated by a modified PCM which considers the effect of annual precipitation differences (PPCM in Section 2.4).

## 2.4. Determining the Bushfire Impact on Water Balance

### 2.4.1. Paired Catchment Method (PCM)

The PCM assumes that in two paired catchments, similar in climate, vegetation cover, and catchment properties, the correlation between their streamflow will remain the same if their vegetation cover remains the same. Suppose one is designated to be the burned catchment (b) and the second is the unburned donor catchment (also known as control catchment, c). Before bushfires, annual streamflow in catchment b ( $Q_b$ ,  $\text{mm yr}^{-1}$ ) can be

simulated by the annual streamflow in catchment c ( $Q_c$ ) using a linear regression model (Bren & Lane, 2014; Brown et al., 2005; Hornbeck et al., 1993):

$$Q_b = Q_{b,\text{sim}} + \epsilon = \alpha Q_c + \beta + \epsilon \quad (4)$$

where  $Q_{b,\text{sim}}$  is the simulated annual streamflow in catchment b, and  $\epsilon$  is the model error (or residual,  $\text{mm yr}^{-1}$ ).  $\alpha$  is the coefficient, and  $\beta$  is the interception of the linear regression model.

After bushfires (or other treatments, e.g., afforestation and deforestation), the difference between observed fire-impacted streamflow ( $Q_b$ ) and the simulated unimpacted streamflow in burned catchment b ( $Q_{b,\text{sim}}$ , learned from pre-fire data) is considered as the fire effects on  $Q$  ( $\Delta Q_{\text{fire}}$ ,  $\text{mm yr}^{-1}$ ):

$$\Delta Q_{\text{fire}} \approx Q_b - Q_{b,\text{sim}} \quad (5)$$

Coefficient of determination ( $R^2$ ) is used for indicating the fraction of explained variance of the linear regression model:

$$R^2 = 1 - \frac{\text{SSE}}{\text{SST}} = 1 - \frac{\sum_{i=1}^n |y_i - \hat{y}_i|^2}{\sum_{i=1}^n |y_i - \bar{y}|^2} \quad (6)$$

where SSE is the sum of squares of the model error and SST is the total sum of squares,  $y_i$  are the observed values of the variable of interest,  $\hat{y}_i$  are the predicted values,  $\bar{y}$  is the mean of the observations, and  $n$  is the number of years.

#### 2.4.2. Precipitation-Corrected Paired Catchment Method (PPCM)

The experiment design of PCM mainly uses small and adjacent catchments with similar climates and vegetation cover, which lead to similar streamflow processes. Though median-sized catchments (mostly 100–500 km<sup>2</sup>) are different in size from the experiment design and their distance may also increase, the concept of PCM can still be useful for examining the similarity between the two catchments (e.g.,  $R^2$  and  $\epsilon$  in linear regression) and determining the fire effects. As the size of catchments and their distances increase, there can be some differences in their annual precipitation ( $DP_{b,c} = P_b - P_c$ ,  $\text{mm yr}^{-1}$ ), which may bring some differences in streamflow under similar vegetation cover. In this case, we assume that  $DP_{b,c}$  can partially explain the variations of  $Q_b$  and reduce  $\epsilon$ , while using PCM analysis for these median-sized catchments (Figure S12b in Supporting Information S1).

Therefore, we proposed a modified form of PCM to consider the effect of the annual precipitation differences (PPCM):

$$Q_b = Q_{b,\text{sim}} + \epsilon = \alpha_1 Q_c + \alpha_2 DP_{b,c} + \beta + \epsilon \quad (7)$$

where  $\alpha_1$  and  $\alpha_2$  are the coefficients,  $\beta$  is the interception, and  $\epsilon$  denotes the residual of the two-variable linear regression model.

To avoid over-fitting, step regression is used to test if the consideration of each two variables ( $Q_c$  and  $DP_{b,c}$ ) in the linear regression is statistically effective for predicting  $Q_b$ . Only variables that help to reduce Akaike Information Criterion (AIC) (Venables & Ripley, 2002) are eventually included in the linear regression model of PPCM (Equation 7).

A sensitivity analysis was conducted to test the hypothesis that the accuracy of PCM can be improved by considering the influences of  $DP_{b,c}$  as illustrated by PPCM. The catchments selected in this study are mostly of medium size and in a median distance to each other (usually less than 100 km). Using 27-year (1982–2008) pre-fire streamflow data of all 19 catchments, 135 possible paired relationships were constructed (without trend in  $\epsilon$  during calibration, which may lead to considerable biases in predictions, Figure 3). In the majority of these relationships (85%), we found that adding  $DP_{b,c}$  to the original PCM reduced the error statistic AIC in predicting  $Q$  (Figure 4a) and then included it in the PPCM. The improvements were also illustrated by comparing the  $R^2$  of PCM and PPCM (Figure 4b), although it tends to be smaller when a higher  $R^2$  has been achieved by PCM. Overall, the proportional increases in  $R^2$ , as compared to all possible improvements ( $1 - R^2$ ), range from 0% to 71%.

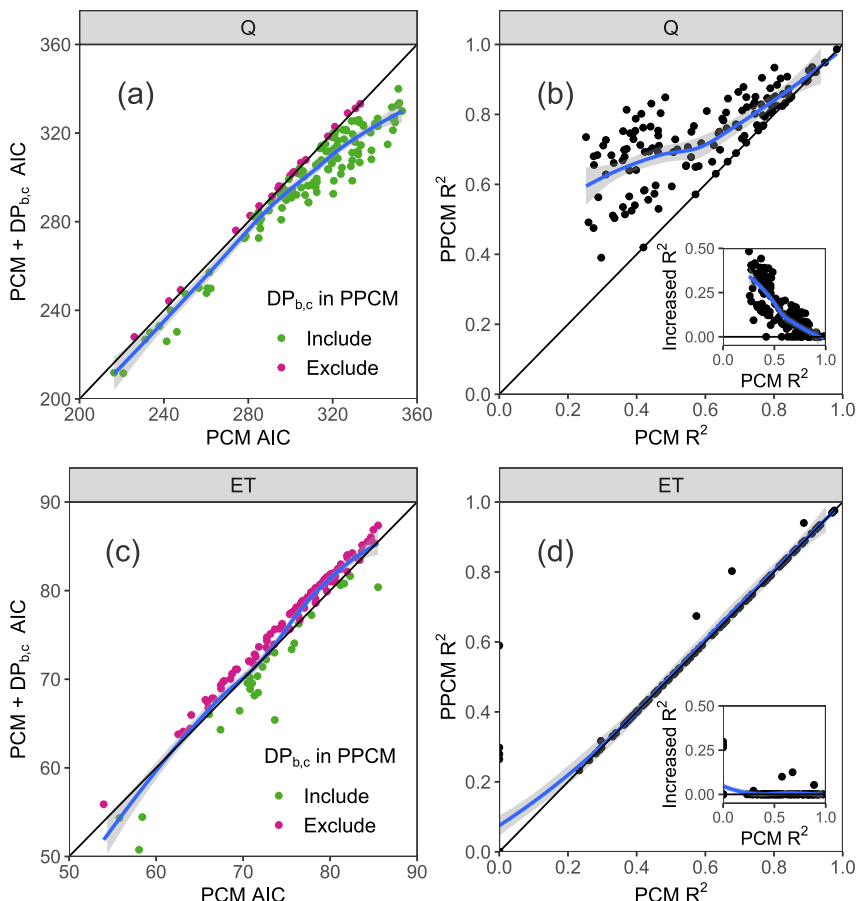


**Figure 4.** (a, c) Analyzing the benefit of using annual precipitation differences ( $DP_{b,c}$ ) in Precipitation-corrected Paired Catchment Method (PPCM) based on the change in Akaike Information Criterion and (b, d) comparing the  $R^2$  between Paired Catchment Method (PCM) and PPCM for all possible paired catchments. The improvements of PPCM to PCM are also shown in the increased  $R^2$  between the two methods. The local regression curves are depicted for scattered points in each panel.

#### 2.4.3. Determining the Fire Impact on ET and $\Delta S$

Although paired catchment analysis is mainly designed for streamflow analysis, it can also be applied for analyzing ET changes. It is noted that the catchment-scale ET is not directly available from field measurements, but obtained from ET modeling. As illustrated in this study, the ET data were produced by the PML-V2 model mainly with remotely sensed LAI and climate forcing and were validated against the site-scale measurements (see details in Section 2.2). To isolate the fire effects on ET, the modeled data were analyzed using PPCM with a similar two-variable linear regression model that simulates ET without fire effects ( $ET_{b,\text{sim}}$ ,  $\text{mm yr}^{-1}$ ). Before bushfires, the annual ET in the burned catchments ( $ET_b$ ) can be simulated using the ET in the control catchment ( $ET_c$ ) and their annual precipitation differences ( $DP_{b,c}$ ).

$$ET_b = ET_{b,\text{sim}} + \epsilon = \alpha_1 ET_c + \alpha_2 DP_{b,c} + \beta + \epsilon \quad (8)$$

where  $ET_{b,\text{sim}}$  is the simulated annual ET in catchment b, and  $\epsilon$  is the model error (or residual,  $\text{mm yr}^{-1}$ ).  $\alpha_1$  and  $\alpha_2$  are the coefficients.  $\beta$  is the interception of the linear regression model.

After fires, the difference between the original fire-impacted  $ET_b$  and the predicted unimpacted  $ET_{b,\text{sim}}$  is considered as the fire effects on ET ( $\Delta ET_{\text{fire}}$ ):

$$\Delta ET_{\text{fire}} \approx ET_b - ET_{b,\text{sim}} \quad (9)$$

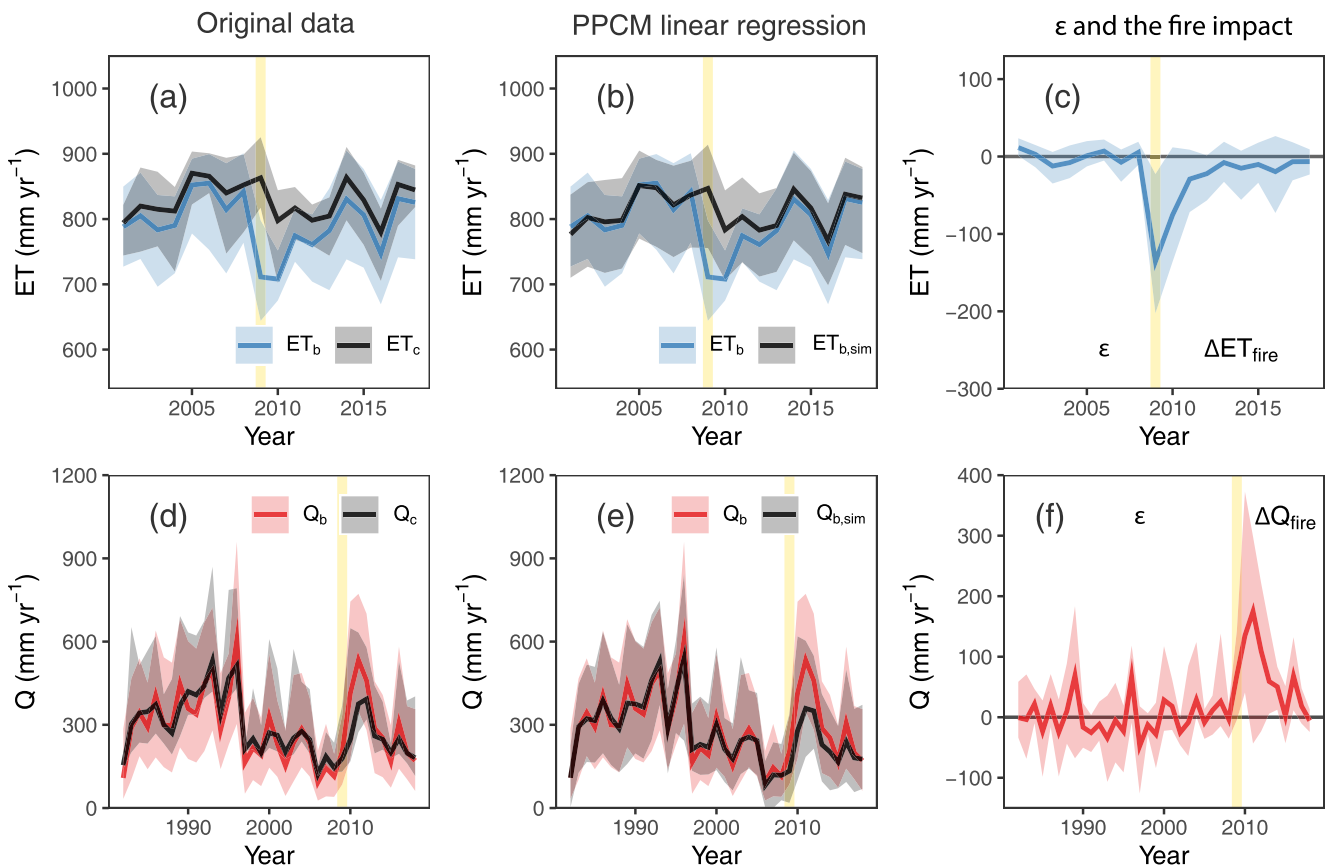


**Figure 5.** Quantification of the bushfire impact on evapotranspiration and streamflow ( $Q$ ). The yellow vertical line indicates the timing of the 2009 Victorian Bushfires. (a, d) Time series of the original data and (b, e) the linear-transformed data based on Equations 7 and 8 in Precipitation-corrected Paired Catchment Method. (c, f) model error ( $\epsilon$ , before bushfires) and the estimated bushfire-induced changes ( $\Delta ET_{\text{fire}}$  and  $\Delta Q_{\text{fire}}$ , after bushfires, 2009–2018). For each panel, thick lines are the mean values among unburned donor catchments (c) and burned catchments (b), respectively, shaded by the minimum-maximum range.

As in estimating  $Q$  changes (Equation 7), the variable  $DP_{b,c}$  is initially kept in Equation 8 to consider its possible influence on simulating  $ET_{b,\text{sim}}$ , especially in drylands where ET is mostly limited by precipitation. To avoid over-fitting, step regression is performed to select the eventual variables based on AIC.

A successful PPCM analysis for ET changes relies on the accuracy of ET data. Therefore, validation of the ET data in describing both ET variability under climate variability and ET response to fires, at least at the site scale (as illustrated in Section 2.2), will be essential to the analysis of the fire effect on ET. In a similar sensitivity test of PPCM using the modeled ET, we found that  $DP_{b,c}$  was mostly (80%) unable to reduce model error (AIC) and excluded it in the eventual formula of PPCM to avoid over-fitting (Figure 4c). This can be attributed to the insensitivity of ET to precipitation in the selected catchments, whose ET is mostly limited by energy (aridity indexes are 0.9–1.1 for 16 of all catchments). Meanwhile, the field measurements of the annual ET for these deep-rooted eucalypt forests were relatively consistent ( $841 \pm 34 \text{ mm yr}^{-1}$ ) between years despite large variation in rainfall (Mitchell et al., 2012), which is attributed due to their ability in accessing deep water in drought period (Talsma & Gardner, 1986). The PML-V2 simulates a similar result as well for unburned catchments ( $829 \pm 28 \text{ mm yr}^{-1}$ , the black line in Figure 5a). For burned catchments, although there are concerns that the fires may have dramatically changed the rooting depth distributions, the previous studies usually ignore the possible changes in deep roots in the most common type of forests in southeast Australia that mostly survive from fires and recover by resprouting (Nolan, Mitchell, et al., 2014; Nolan, et al., 2015; Sun, Meyer, et al., 2020). Overall, the validation results for PML-V2 ET modeling (Figure 2 and Figure S7 in Supporting Information S1) indicate that the simulated ET data are acceptable for estimating ET changes after fires.

Unlike the dramatic differences in ET and  $Q$  after bushfires (Figures S8f and S8g in Supporting Information S1), the differences in  $P$  are insignificant between burned and unburned catchments (Figure S8e in Supporting



climate together drive the changes in variable  $y$ , the contribution of the climate ( $\Delta y_{\text{clim}}$ ,  $\text{mm yr}^{-1}$ ) is computed as follows:

$$\Delta y_{\text{clim}} = \Delta y_{\text{total}} - \Delta y_{\text{fire}} \quad (14)$$

where  $\Delta y_{\text{fire}}$  of each water balance variable is computed in Section 2.4. Contributions are computed at the annual scale and the period scale.

### 3. Results

#### 3.1. Quantification of the Bushfire Impact on ET and $Q$ at an Annual Scale

The bushfire impact on ET and  $Q$  was extracted from the overall impact of climate and fires for the eight burned catchments (Table 2). Through a series of processes for examining the similarity of hydrological fluxes in paired catchment analysis, the optimal donor catchment holds the lowest uncertainty among all possible donor catchments ( $\sigma_{\text{WB}}$ , Figure 3). Although all variables show great inter-annual variabilities, variations are similar between the two groups of catchments in the pre-fire period and the disparities began after the 2009 Victorian Bushfires (Figures 5a and 5d). In pre-fire calibration, the PPCM yields good model results, with  $R^2$  being 0.79–0.97 for  $Q$  and 0.64–0.98 for ET. This indicates the method is suitable for simulating the variations of the two hydrological fluxes before bushfires (Figures 5b and 5e).

Assuming the paired catchment relationship will continue without the occurrence of fires, the model predictions were extended to the post-fire period for simulating the unimpacted state of the two fluxes and the fire effects were separated by the observed fire-impacted fluxes and the predicted unimpacted fluxes (Figures 5c and 5f). In results, the bushfires decrease ET and increase  $Q$  in these burned catchments during the post-fire decade. Overall, the averages of estimated bushfire-induced changes in the two fluxes ( $\Delta ET_{\text{fire}}$  and  $\Delta Q_{\text{fire}}$ ) are much higher than their overall error ( $\sigma_{\text{ET}}$  and  $\sigma_Q$ ) during calibration (4.2 times for ET and 2.4 times for  $Q$  in the ensemble results of all catchments, Table 2). More importantly, the ensemble of the eight fire-impacted catchments generates much smaller  $\sigma_{\text{ET}}$  and  $\sigma_Q$ , compared to those of individual catchments (Table 2). Therefore, in the following sections, we used the PPCM in an ensemble way for quantifying the bushfire impact on ET and  $Q$  at an annual scale.

#### 3.2. Temporal Asynchronization of Bushfire-Induced Changes in Water Balance Components

Based on the model estimates of PPCM, we found that there are asynchronous responses of ET and  $Q$  to bushfires (Figure 6). First, the ET response to the 2009 Victorian Bushfires is direct, causing a  $136 \text{ mm yr}^{-1}$  ET decline when averaged for all catchments during the first year after fires. In particular, there is a  $202 \text{ mm yr}^{-1}$  ET decline for catchment #405231 which suffered the most severe burning (burned area = 89%, Table 2). ET recovered quickly in the subsequent years as the fire effects faded out over time. Overall,  $\Delta ET_{\text{fire}}$  is relatively low for the majority of catchments 5 years after bushfires. It should be noted that the ET in catchment #405231 does not fully recover to a similar level even after a decade, as compared with its donor catchment (Figure S13 in Supporting Information S1).

In comparison with ET, the response of  $Q$  is lagged, with a larger magnitude of changes (Figure 6a). The rising  $\Delta Q_{\text{fire}}$  mostly peaked in the second or third year after bushfires for all burned catchments. Seven of the eight burned catchments have a peak  $\Delta Q_{\text{fire}}$  that is larger than  $100 \text{ mm yr}^{-1}$ . Among them, the maximum  $\Delta Q_{\text{fire}}$  (with an astonishing  $373 \text{ mm yr}^{-1}$ ) occurred in catchment #405209 (burned area = 75%). However, a larger burned area does not essentially cause a larger peak  $Q$  increase. For catchment #405231 (burned area = 89%), the maximum  $\Delta Q_{\text{fire}}$  is just  $209 \text{ mm yr}^{-1}$ . With the lag of  $\Delta Q_{\text{fire}}$ , the recovery process is therefore delayed. But 5 years after fires, the bushfires have a limited impact on  $Q$  (almost no significant points in Figure 6a). The  $\Delta Q_{\text{fire}}$  in 2016 is relatively small ( $0.01 < p < 0.05$ ).

According to our assumption that the bushfire impact on the precipitation is negligible, the bushfire-induced changes in catchment water storage change ( $\Delta S_{\text{fire}}$ ) were derived from the changes in ET and  $Q$  (Section 2.4.3). The ensemble  $\sigma_{\Delta S}$  ( $28.9 \text{ mm yr}^{-1}$ ) was also computed by the overall error of the other two fluxes (Equation 13). Based on the derived  $\Delta S_{\text{fire}}$  data, we surmised that the asynchronous responses of evapotranspiration and streamflow to bushfires occurred with the initial increase, and the later decrease in water storage (Figure 6b). In the first year, the storage increased (on average  $66.4 \text{ mm yr}^{-1}$ ) since the ET decline is larger than the increase in  $Q$ .

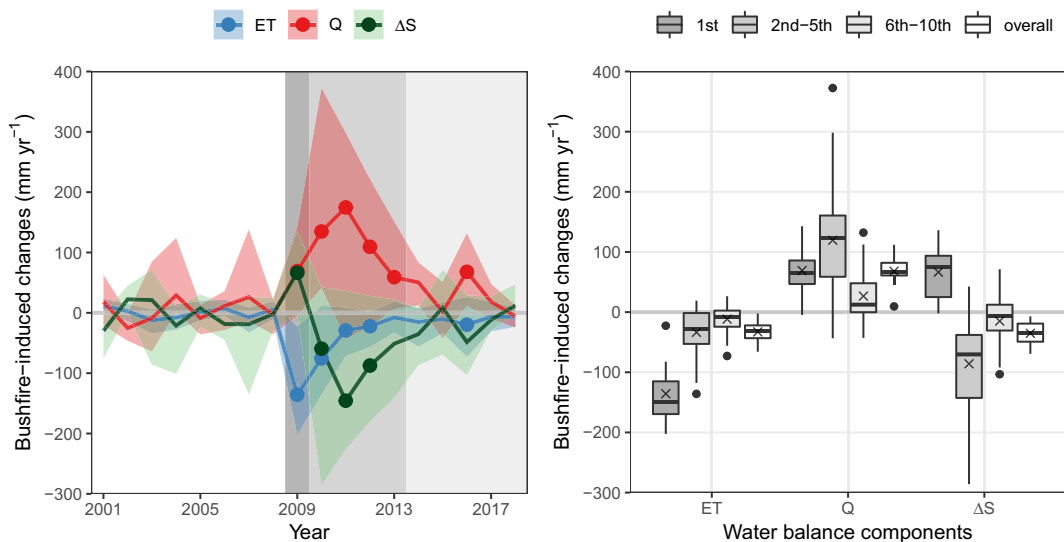


**Figure 6.** Temporal asynchronization of bushfire-induced changes in water balance components, illustrated by (a) time series of changes and (b) boxplots of different periods. The thick lines in panel (a) are the mean values of each variable, shaded by the minimum-maximum range. The pre-fire estimates indicate the uncertainty of the method, and the solid points denote the significant post-fire changes that differ from the pre-fire model error ( $p < 0.05$ ). As the bushfires mainly occurred in early February 2009, we set 2009 as the first event year that received the bushfire impact. The crosses in panel (b) are the mean values for each group.

From the second to fourth year after the fire event, the storage dramatically declined ( $p < 0.05$ , the green points in Figure 6a), caused by the lagged response of increased  $Q$  and the fast recovery of decreased ET. As in ET and  $Q$ , the water storage change is not significant 5 years after the fires ( $p > 0.05$ ). Overall, these results indicate that the bushfire impact on water balance tends to diminish to a low level 5 years after fires.

Aggregating the model estimates for the post-fire period (2009–2018, Table 2), we found that the bushfire caused  $33 \pm 20 \text{ mm yr}^{-1}$  ET declines (mean  $\pm$  standard deviation),  $68 \pm 32 \text{ mm yr}^{-1}$  increases in  $Q$  (Figure 6b). Therefore, the bushfires may have induced  $35 \pm 22 \text{ mm yr}^{-1}$  water storage declines averaged for all catchments. Since the long-term  $Q$  increases hugely exceed the ET decreases especially during high precipitation years, approximately half (52%) of streamflow increases may occur with a reduction in catchment water storage, indicating that less water was stored after bushfires under the same amount of precipitation.

### 3.3. Relationship Between Burned Area and Bushfire-Induced Water Balance Changes

At the catchment scale, the bushfire-induced water balance changes are related to the fraction of the burned area. Overall, the decade-averaged  $\Delta ET_{\text{fire}}$  and  $\Delta Q_{\text{fire}}$  are significantly linearly correlated to the burned area ( $p < 0.05$ ,  $R^2 = 0.87$  and  $R^2 = 0.66$ , Figure 7a). The unexplained variance is likely to link with other factors, including burned severity, recovery trajectory of vegetation, and the topography setting for runoff production. However, the relationship between the decade-averaged  $\Delta S_{\text{fire}}$  and the burned area is not well explained by the linear model at the catchment scale ( $p > 0.05$ ), indicating a more complex nature of water storage change after bushfires. Even so, we found that the catchments with a high burned area (burned area  $> 70\%$ ) have noticeably larger decade-averaged storage declines than that of catchments with moderate/low burned area (Figure 7b,  $-45.3 \text{ mm yr}^{-1}$  vs.  $-34.7/-7.1 \text{ mm yr}^{-1}$ ).

### 3.4. The Contributions of Bushfires and Climate in Post-Fire Water Balance Changes

Based on the PPCM estimates, the contributions of bushfires to overall post-fire water balance changes were compared with that of climate variability (Figure 8). Overall, our results indicate that the bushfires dominated the decade-averaged ET changes ( $\Delta ET_{\text{total}}$ ) and ET variabilities for the first 3 years. For the majority of catchments, the bushfires also played a more important role than the climate variability in the  $Q$  changes ( $\Delta Q_{\text{total}}$ ). For example,  $Q$  increased by 162% compared with the pre-fire average in the year 2010 for catchment #405209,

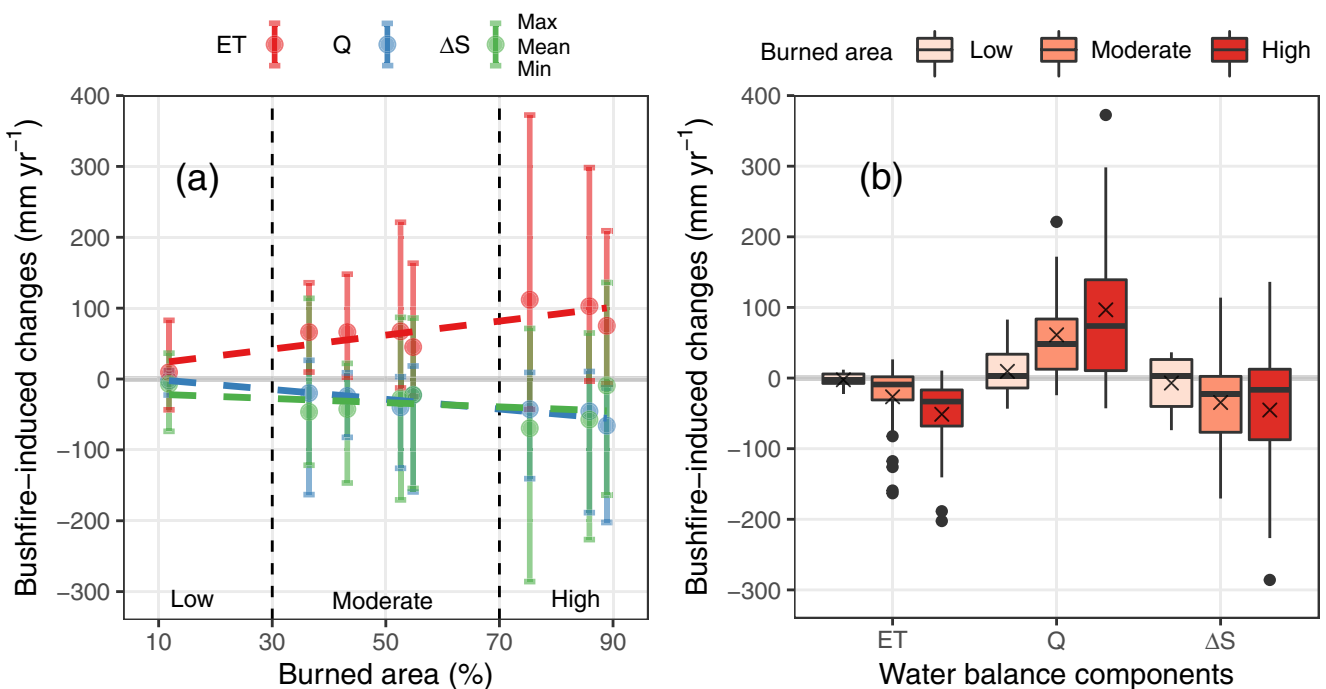


**Figure 7.** Relationship between burned area and bushfire-induced changes of water balance components based on (a) linear regression at the catchment scale and (b) relative comparison between decade averages of different burned area groups. In panel (a), the colored dashed lines are fitted by linear regression models for the three water balance components. In panel (b), the crosses are the mean values for each group. The decade averages of bushfire-induced changes in ET and  $Q$  have significant linear relationships with burned area ( $p < 0.05$ ,  $R^2 = 0.87$  and  $R^2 = 0.66$ ). For  $\Delta S$ , the linear relationship is not significant at the catchment scale.

and 81% of the  $Q$  increase is attributed to bushfires. Overall, as the catchments recovered from the bushfires, the contributions of bushfires to the annual variability approached a low level.

On a long-term basis, the bushfires explained  $85 \pm 20\%$  (mean  $\pm$  standard deviation) of decade-averaged ET deceases and  $60 \pm 28\%$  of  $Q$  increases for all burned catchments (Table 2, Figure 8d). In seven of the eight burned catchments, the decadal storage increases caused by a wetter climate are partially reduced by the bushfire-induced storage loss (10%–63% in range, Table 2). The overall result indicates that the fire impact on hydrological partitioning may have offset 43% of the expected impact of precipitation increases on water storage during a wetter climate for these catchments (Table 2).

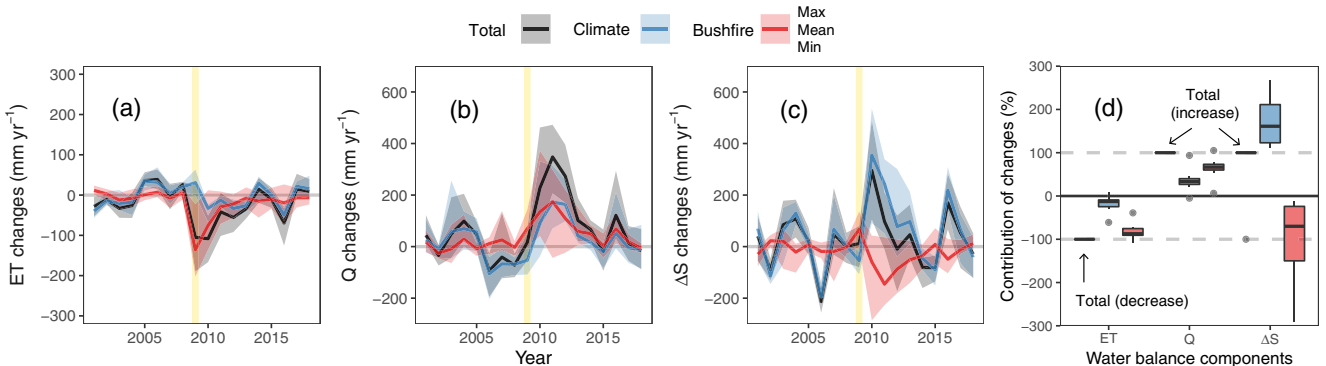


**Figure 8.** Contributions of bushfires and climate on (a–c) inter-annual variability of water balance components (ET,  $Q$ ,  $\Delta S$ ) and (d) the average changes for the postfire decade. The yellow vertical lines indicate the timing of the 2009 Victorian Bushfires. In panel (d), the boxplot of overall changes shrinks into one black segment to indicate the polarity (100% or –100%, increase or decrease).

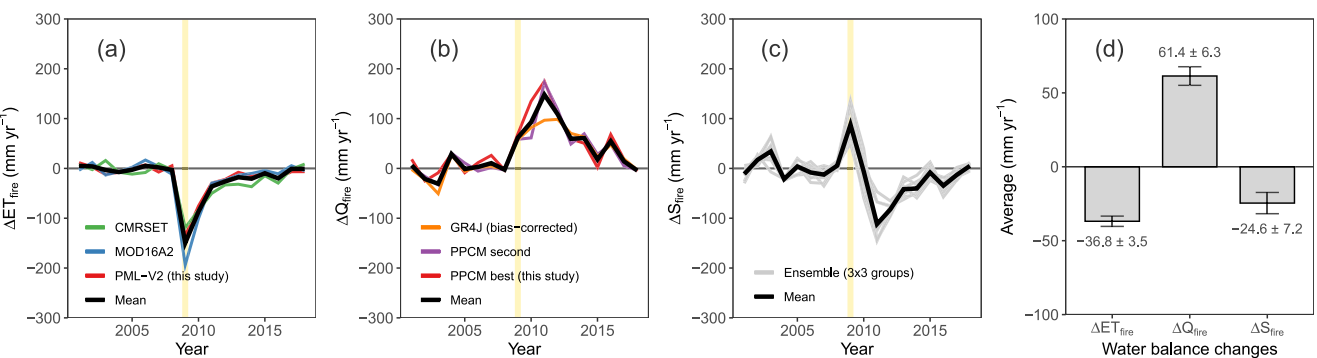


**Figure 9.** Estimated fire-induced water balance changes averaged for all burned catchments using independent data/methods. (a–c) Time series and (d) the average results for the postfire decade. The yellow vertical lines indicate the timing of the 2009 Victorian Bushfires. The ensemble in panel (c) is from the nine combinations of the evapotranspiration (ET) estimates from the three ET products in panel (a) and the three kinds of  $Q$  estimates in panel (b). The error bars shown in panel (d) are computed by the results of panels (a–c), respectively.

## 4. Discussion

### 4.1. Uncertainty of Estimating Bushfire-Induced Water Balance Changes

In this study, we explored if the PCM can be used for medium-sized basins ( $\sim 100\text{--}500 \text{ km}^2$ ) and considered the overall changes in the three catchment water balance components, including ET,  $Q$  and  $\Delta S$ . Though the increase in catchment size and their distances can increase model uncertainty, we found that the PPCM generally yields satisfactory results. The estimated fire impact on ET and  $Q$  is mostly significantly different from the model error as indicated by the pre-fire data. To our knowledge, this is the first attempt to extend the use of PCM (a) in estimating streamflow changes by considering annual precipitation differences between paired catchments, and (b) from the simple comparison of streamflow to a more fulsome investigation of the overall catchment water balance.

While benefiting from such intention, uncertainty still comes from both the data and the method. As  $Q$  is observed for the catchment, the data error mainly comes from the remotely-sensed ET estimates (with a diagnostic ET model PML-V2). Although we evaluated the model's ability in describing ET responses to fires at a site scale (AU-Wac), more test work is required to fully answer if current high-resolution ET data, driven by satellite images and climate forcing, can capture the basic feature of ET changes after fires across other parts of the world. There are also errors in estimating ET and  $Q$  changes in PPCM, which would inevitably propagate to the estimation of  $\Delta S$ . Meanwhile, it is worthwhile to use other alternative data/methods as references to test the bushfire impacts, though they may be less performed in the accuracy of the data or may require bias correction in estimations.

First, we tested if the PPCM method is overall robust in predicting ET and  $Q$  under natural climate variability in a changing climate. We used several sets of two unburned paired catchments (without fire impact) as a reference for data error and checked if there are noticeably increased model errors in post-fire estimations during 2009–2018. In practice, the PPCM was implemented for searching the possible donor catchment for each of the 11 unburned catchments. Among them, six independent paired catchment relationships show a similar range of overall error ( $\sigma_{WB} = 44\text{--}82 \text{ mm yr}^{-1}$ , ensemble  $\sigma_{WB} = 33.2 \text{ mm yr}^{-1}$ , Table S1 in Supporting Information S1) as the result of burned catchments ( $\sigma_{WB} = 30\text{--}77 \text{ mm yr}^{-1}$ , ensemble  $\sigma_{WB} = 35.6 \text{ mm yr}^{-1}$ , Table 2). While constructing their study/donor relationships, the donor catchments that are previously used in Table 2 (e.g., catchments #226204, #226220) are preferred to be set as the donor catchments (Table S1 in Supporting Information S1). We found that the post-fire error ( $\epsilon_{post}$ ) fluctuates around the zero line as it did in pre-fire data (Figures S14c and S14f in Supporting Information S1). The mean  $\epsilon_{post}$  for estimating ET and  $Q$  changes are  $3.38$  and  $2.73 \text{ mm yr}^{-1}$ , indicating that the PPCM is overall robust in predicting average post-fire changes in ET and  $Q$ .

Second, we explored if other high-resolution ET products (MOD16A2 and CMRSET, see Section 2.2) have similar estimations of  $\Delta ET_{fire}$ . As these ET data may have used different climate forcing,  $\Delta ET_{fire}$  were extracted by simply comparing ET anomalies between burned catchments and their optimal donor catchments (with lowest  $\sigma_{ET}$ , Figure S15 in Supporting Information S1). It indicates the overall results of the other two ET products have similar ET variations to that of PML-V2 with fast recovery of ET during the first 3 years (Figure 9a), though

the ET decline is more dramatically for the first year after fires using MOD16A2 and ET is less recovered in 5 years after bushfires using CMRSET. Overall, MOD16A2 and CMRSET estimate that ET decreased by 38.5 and 39.2 mm yr<sup>-1</sup>, respectively. In comparison, the result of PML-V2 is 32.8 mm yr<sup>-1</sup>. The standard deviation for the three methods is 3.5 mm yr<sup>-1</sup>.

Third, we explored if other data/methods have similar estimations of  $\Delta Q_{\text{fire}}$ . Here, the ranked second most satisfying donor catchment in the hydrological similarity to the burned catchment (examined by PPCM,  $\sigma_{\text{WB}} = 44\text{--}100 \text{ mm yr}^{-1}$ , ensemble  $\sigma_{\text{WB}} = 39.4 \text{ mm yr}^{-1}$ , Table S2 in Supporting Information S1), can also be set as the donor catchment for quantifying the fire impacts on  $Q$  (Figure S16 in Supporting Information S1). Using this set of paired catchments, the PPCM estimates that  $Q$  averagely increased by 60.7 mm yr<sup>-1</sup> during the post-fire decade. ET decreased by 33.1 mm yr<sup>-1</sup>, which is almost the same as that of the optimal donor catchments (32.8 mm yr<sup>-1</sup>, Table 2). Meanwhile, a widely-used hydrological model in Australia, that is, GR4J (Ficchi et al., 2019; Perrin et al., 2003), was used for estimating the unburned flow and quantifying the fire impact on  $Q$  as the differences between observed burned flow and modeled unburned flow (observation-modeling scheme). The GR4J model was calibrated for 1982–2004 which covers both wet and dry periods and was used for predicting unburned streamflow for 2005–2018 (Section S1 in supplement). Using the same eight burned catchments and seven unburned donor catchments, we found that the GR4J model has systematic model biases, which becomes most prominent in 1997 when the regional climate shifted to the Millennium Drought (blue line in Figure S17a in Supporting Information S1). As the system bias seems to be stable during the drought period 2005–2008, the overall results were removed mean of that period. However, the system bias in the post-fire period is still largely unknown, as there seems to be a continuously dropping system bias since 1997 ( $\epsilon_{\text{post}}$  in Figure S17a in Supporting Information S1). Using the same seven unburned/donor catchments in Table 2 and Table S1 in Supporting Information S1 to indicate the possible post-fire system bias (no fire effects), we found there is an overestimate of modeled unburned streamflow and therefore an underestimate of the fire impact during the post-fire decade (on average  $-12.5 \text{ mm yr}^{-1}$ ). The overestimation of unburned streamflow may be related to the fact that the runoff regimes in these watersheds are not recovered after a long period of drought (1997–2008) (Peterson et al., 2021). This system bias of the conceptual model GR4J in describing the non-stationary streamflow in huge climate variability indicates the importance of physical mechanisms in hydrological models (Saft et al., 2016; Stephens et al., 2019). In this case, we assumed that the system biases of the burned catchments are similar to those of unburned catchments at the decade scale. Therefore, the result of GR4J was bias-corrected and estimated that there is an overall 55.5 mm yr<sup>-1</sup>  $Q$  increase during the post-fire decade (Figure S17b in Supporting Information S1).

Eventually, there are three independent results for estimating ET and  $Q$  changes using independent data/methods (Figures 9a and 9b). Time series of the fire-induced water storage change are also deduced by possible combinations between the results of ET and  $Q$  to indicate the ensemble mean and the model error (9 groups created, Figure 9c). In general, the ensemble results show that ET averagely decreased by  $36.8 \pm 3.5 \text{ mm yr}^{-1}$  (mean  $\pm$  standard deviation, between the three data/methods) and  $Q$  averagely increased by  $61.4 \pm 6.3 \text{ mm yr}^{-1}$ , indicating there could be a  $24.6 \pm 7.2 \text{ mm yr}^{-1}$  fire-induced water storage decline (the propagated error are calculated using that of other two fluxes, Equation 13) when averaging for all catchments during the post-fire decade 2009–2018. As the results of these independent data/methods converge both at an annual level and at the decade-average level, the overall uncertainty due to method/data selection in estimating bushfire-induced water balance changes should be comparatively small. Therefore, we indicated that the major finding of this study would be overall reliable, which reveals that (a) the reduced evapotranspiration and the increased streamflow due to the 2009 Victorian Bushfires are temporally asynchronous, and (b) there are possible fire-induced water storage changes in burned catchments (Figure 9).

#### 4.2. Bushfire-Induced Vegetation Changes and Hydrological Responses

Major bushfires are relatively common in southeast Australia's temperate broadleaf forests that are dominated by eucalypts (Boer et al., 2020; Kuczera, 1987; Langford, 1976). However, eucalypts have special fire-adaptive traits, including resprouting after fires, which make them well-adapted to the local fire regime (Christina et al., 2011; Crisp et al., 2011; Nolan et al., 2015). In this study, the catchment-scale leaf area, drastically dropped by more than 50% with high burned severity and burned area in the fire event, but can quickly recover to more than 80% within less than 5 years as compared with their donor catchments (Figure S1f in Supporting Information S1).

Previous studies generally reported a fast recovery of LAI for the first 2–3 years after fires in these fire-resilient eucalyptus forests (Heath et al., 2016; Qin et al., 2022).

Bushfires can modify the partitioning of evaporative and runoff fluxes, resulting in reduced transpiration and interception, and higher runoff (Boisrame et al., 2019; Kumar et al., 2021; Wine, Cadol, & Makhnii, 2018). The ET changes are usually attributed to the change of stand structure, readily leading to a decline in ET as a result of less intercepted and transpired water from the canopy, which exceeds the increased soil evaporation (illustrated by Figures 11b and 11d) (Gharun et al., 2018; Montes-Helu et al., 2009; Morison et al., 2020; Nolan et al., 2015; Poon & Kinoshita, 2018; Roche et al., 2018). Other forces may be related to the soil moisture condition, such as the increase of constraints from post-fire soil water (Kettridge et al., 2014) and the role of scale-specific connectivity (Depante et al., 2019; Hallema et al., 2017). However, the deep-rooted mixed species eucalypt forests, which have a low mortality rate after fires and recover via resprouting, often maintain similar rates of sap transpiration under wet and dry conditions due to their ability in accessing deep water (Mitchell et al., 2012; Nolan et al., 2015; Talsma & Gardner, 1986). But for ash-type forests, which usually die after severe fires and recover via seedlings, the distribution of root depth may change. The recovering young ash forests from seedlings, though less common in southeast Australia compared with recovery via resprouting, would require time for spreading roots to reach a mature root distribution. However, such changes in roots may also relate to the changes in stand structure, that is, LAI and sapwood, which are generally attributed to be a major factor that drives the change of transpiration and interception after bushfires (Nolan, Mitchell, et al. 2014; Nolan, et al., 2015; Sun, Meyer, et al., 2020). As a result, the diagnostic PML-V2 ET model using the remotely-sensed LAI has the potential to describe the response of ET to bushfires, which was illustrated by the good validation result against site observations (Figure 2). At the catchment scale, the estimated ET changes by PML-V2 ET data and PPCM show a high linear correlation with the LAI changes ( $R^2 = 0.93$ , Figure 10b). The overall recovery trajectory of ET in this study is also similar to the empirical result that reports ~20% ET reductions during the first year in high severity sites which takes 8–12 years for full recovery (Figure 7 in Nolan et al., 2015). Even so, the current remote-sensing-based ET model may need to be more widely tested, and further improved by enhancing resolution (such as in describing LAI changes) and representing plant physiological mechanisms (such as the differences in water use between canopy and understory).

The streamflow increases after bushfires are usually attributed to (a) the decrease of ET due to vegetation removal leaving more water for runoff generation (Atchley et al., 2018; Boisrame et al., 2019), and (b) the fire impact on the soil hydraulic properties, which reduces the infiltration and increases surface runoff (Letey, 2001; Shakesby & Doerr, 2006). The decrease in plant water uptake and canopy interception is expected to increase the unsaturated water storage and recharge in the first few years after bushfires, leading to higher streamflow (illustrated by Figure 11b) (Silberstein et al., 2013). Meanwhile, the change in the soil hydraulic properties after severe bushfires, though can decline dramatically in the first few years, may also contribute to the  $Q$  increase. Among these properties, increased soil water repellency, extreme soil drying, reduced soil structure, and soil sealing by ashes after bushfires usually lead to reduced infiltration capacity and reduced soil water capacity in burned hillslopes (Larsen et al., 2009; Nyman et al., 2011, 2014; Sheridan et al., 2007). Therefore, the infiltration-excess overland flow is recorded as the most common type of surface runoff production that responds to bushfires, while saturation excess overland flow was hardly recorded in these forests (Lane et al., 2004). With high-intensity rainfall during high precipitation years, the lower interception and lower infiltration capacity in burned hillslope can dramatically increase overland flow (illustrated by Figure 11d), stimulating the surge of high flow and flash floods (Kean et al., 2011, 2012; Lane et al., 2004; Liu et al., 2022; Versini et al., 2012).

The relative roles of post-fire changes in vegetation cover and soil hydraulic properties in driving different catchment streamflow changes, are still largely unknown within a year and in different years. For example, during the high precipitation years in 2010 and 2011 (Figure 10c), the dramatic increase in  $Q$  may be both related to (a) the increased groundwater storage from the earlier accumulated ET decline and (b) the increased overland flow due to some remaining influences of reduced infiltration capacity. In general, we found that the fire-induced  $Q$  increases are significantly linear-correlated with the P anomalies ( $p < 0.01$ ,  $R^2 = 0.40$ , Figure 10d), indicating the important role of climate in modulating the bushfire impacts and controlling the timing of changes (Maina & Siirila-Woodburn, 2020). But overall, based on the test of significant changes of this study (Figure 6a), the fire effects on water balance tend to diminish to a low level 5 years after fires, which is possibly due to the major recovery of vegetation and soils.

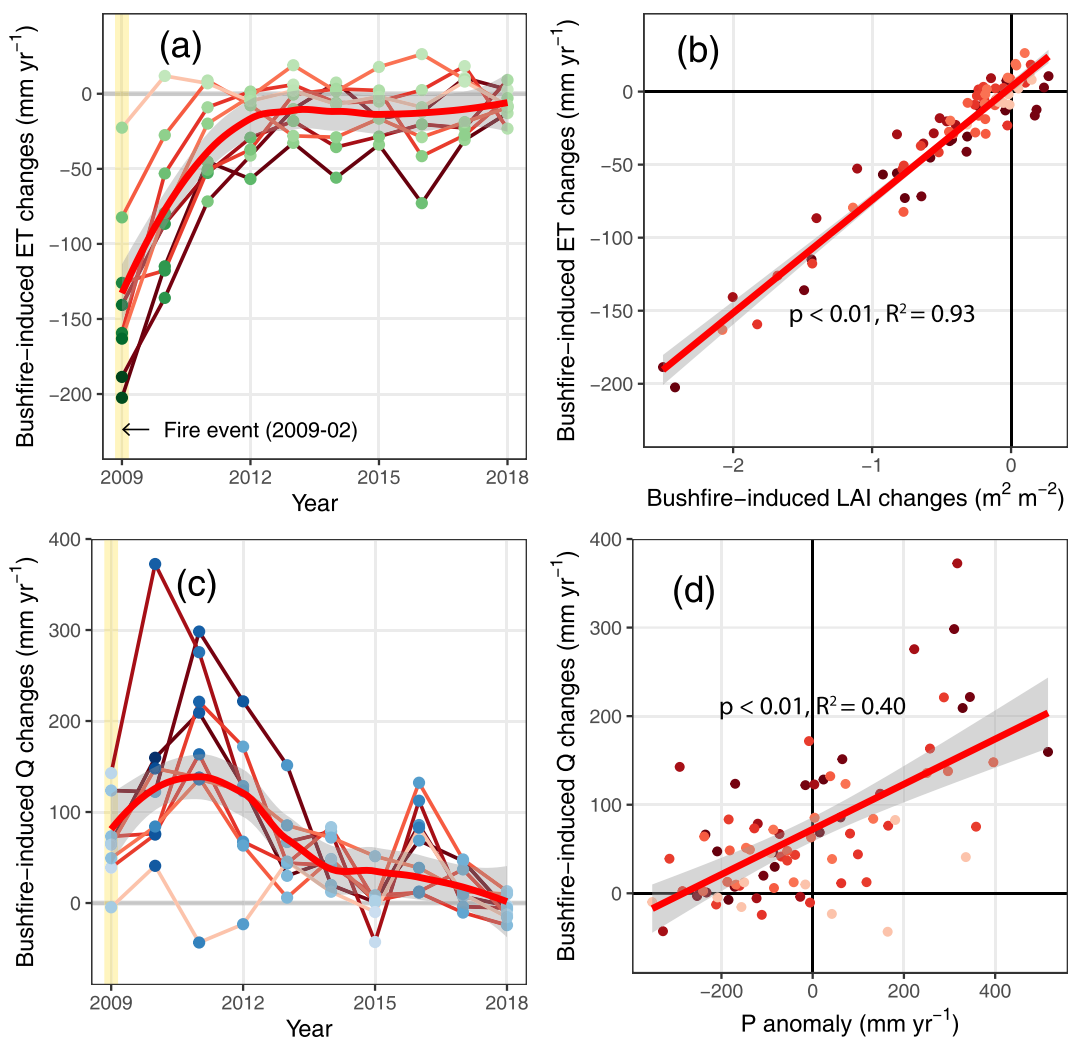


**Figure 10.** (a–b) The dominant role of leaf area index (LAI) changes on estimated evapotranspiration changes and (c–d) the role of precipitation on estimated  $Q$  changes after the bushfire. The thin lines in panels (a and c), as well as the dots in panels (b and d), are grouped by each catchment and filled in different shades of red color to indicate different percentages of burned area. The thick red lines in panels (a and c) are generated by local weighted regression models for all dots to indicate the non-linearity of bushfire impact. The thick red lines in panels (b and d) are generated by linear regression models for all dots.

#### 4.3. Post-Fire Catchment Water Storage Changes in a Changing Climate

The catchment water storage, including surface water and subsurface soil water and groundwater, reflects the differential change of the hydrological partitioning between ET and  $Q$ . In the results, we showed that the bushfire-induced water storage change ( $\Delta S$ ) is hugely impacted by the balancing relationship between decreased ET and increased  $Q$ , which may be modulated by the climate variability (Figure 11). During a dry climate, water storage can increase as the ET decline dominates the change of water balance (Atchley et al., 2018), which then increases  $Q$  as well due to more water are available for subsurface flow (Figure 11b). However, during a wet climate, water storage can comparatively decline when the increase of  $Q$  exceeds the decrease of ET, which means the runoff production is not fully dependent on the increase of soil water storage during the decrease of ET. In this case, the exceptional increase in  $Q$  may be related to the reduced infiltration capacity after bushfires and is activated by high-intensity rainfall during wet climate, leading to more overland flow (Figure 11d). Though the fire impact on interflow and baseflow may be unknown as the fires may promote/suppress these processes via other mechanisms (Nyman et al., 2014; Stoff et al., 2014). Overall, there seems to be a tipping point of climate that drives different water balance changes where increased  $Q$  competes with reduced ET in post-fire forests, which inevitably changes the water storage (Figures 11b and 11d) (Atchley et al., 2018). In this study, as the

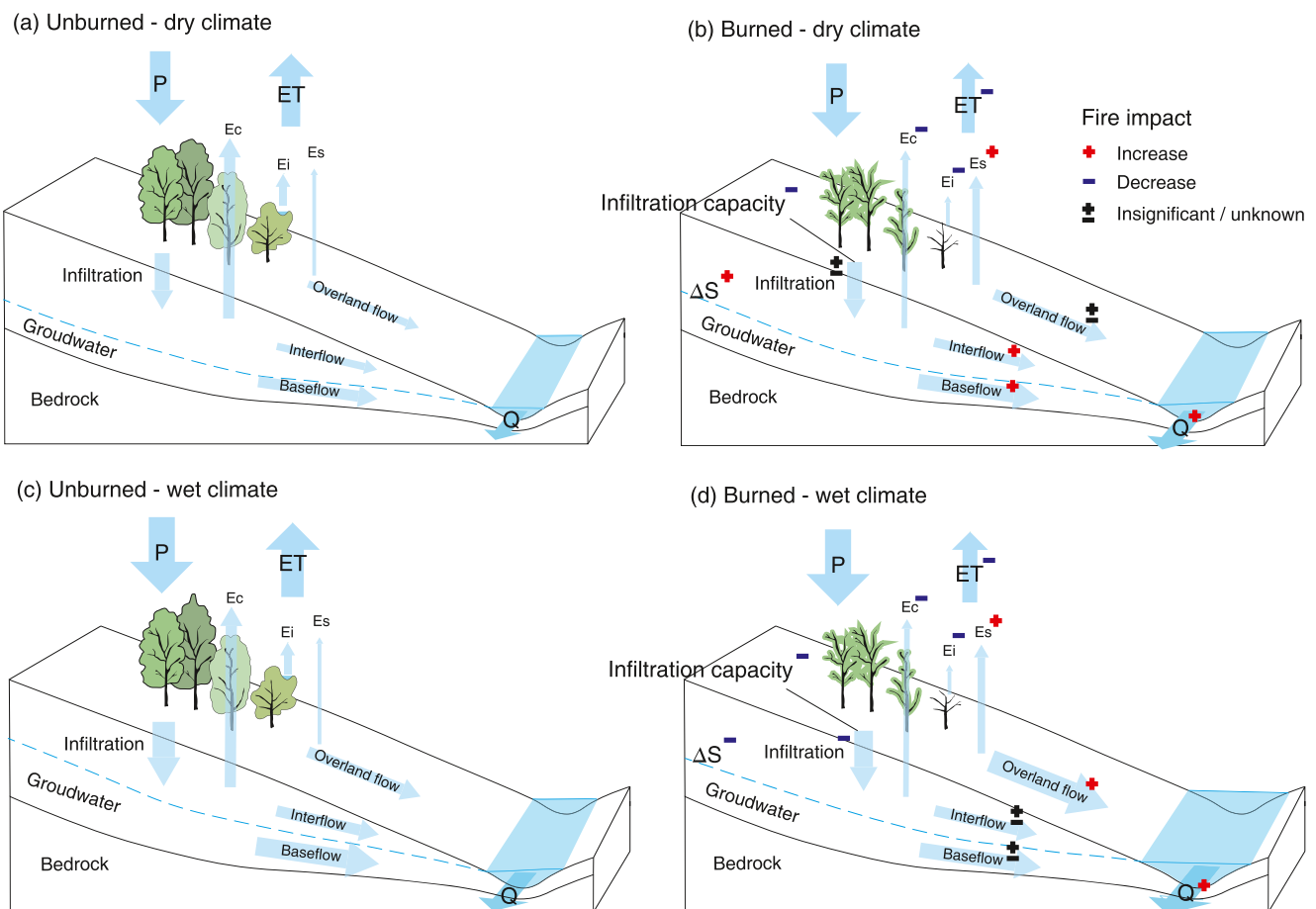


**Figure 11.** Conceptualized mechanisms for explaining the fire impact on hydrological partitioning in a changing climate. The fire impact is illustrated by comparing burned and unburned hillslopes (a–d). The role of climate variability in modulating fire impact is illustrated by comparing burned hillslopes under dry and wet climates (b and d).  $E_c$ ,  $E_s$ , and  $E_i$  denote transpiration, soil evaporation, and evaporation of canopy interception, respectively.

first few years after bushfires are an overall wet period (blue color, Figure 10c), the comparative water storage decline in burned catchments may be mainly related to the decrease of infiltration after bushfires, which exceeds the influence of reduced evapotranspiration on water storage. But in a dry climate and if without high-intensity rainfall, this may not occur as the reduced infiltration capacity rarely stimulates overland flow, especially for a region where the surface runoff is mostly generated by infiltration excess.

## 5. Conclusions

This study modifies the traditional PCM by considering the partial effect of annual precipitation differences between the paired catchments and then uses the modified method for estimating the changes in different catchment water balance components. In the application to the burned catchments and their donor catchments after the 2009 Victorian Bushfires, we found that the decreased evapotranspiration and the increased streamflow due to bushfires are temporally asynchronous, as evapotranspiration gradually recovered since the fire event year and the streamflow may require both accumulated evapotranspiration decline and rainfall extremes to rise to the peak changes (mostly in the second or third year). With continuous recovery, the fire effects tend to diminish to a low level 5 years after fires. Overall, the catchment that suffered from a higher percentage of fire disturbance tends to experience a larger water balance change.

The asynchronous responses of evapotranspiration and streamflow to bushfires indicate that there is a noticeable change in catchment water storage at the annual scale. Our results show that the water storage is initially increased due to the strong evapotranspiration decrease in the first year, while a subsequent decrease in water storage

could be seen with the increase in streamflow during the subsequent two to 3 years. Averaged for the post-fire decade, there seems to be a decline in terrestrial water storage for burned catchments relative to unburned catchments. Consequently, the water storage increase in a wetter climate may be less than expected for these burned catchments.

While we illustrate that there is a potential for using remote sensing data to detect fire effects on water balances, the modified PCM needs to be more widely tested, especially in arid and semi-arid regions where precipitation is a primary limitation on evapotranspiration. It is expected that the increasing accuracy of water balance data and the continuous improvements of such data-based methods, can advance our understanding of hydrological changes in this more fire-prone planet.

## Data Availability Statement

All data used in this study are available from the websites as follows: SILO climate data (<https://www.longpaddock.qld.gov.au/silo/gridded-data/>); GLDAS 2.1 climate data ([https://developers.google.com/earth-engine/datasets/catalog/NASA\\_GLDAS\\_V021\\_NOAH\\_G025\\_T3H](https://developers.google.com/earth-engine/datasets/catalog/NASA_GLDAS_V021_NOAH_G025_T3H)); streamflow data (HRS gauges, <http://www.bom.gov.au/water/hrs/>, non-HRS gauges, <http://www.bom.gov.au/waterdata/>); LE flux data (FLUXNET2015, <https://fluxnet.org/data/fluxnet2015-dataset/>, OzFlux (flux site AU-Wac), <https://data.ozflux.org.au/portal/pub/viewColDetails.jspx?collection.id=1882706%26collection.owner.id=304%26view-Type=anonymous>); GRACE JPL RL06 mascon data ([https://grace.jpl.nasa.gov/data/get-data/jpl\\_global\\_mascons/](https://grace.jpl.nasa.gov/data/get-data/jpl_global_mascons/)); MODIS MCD64A1 burned area data ([https://developers.google.com/earth-engine/datasets/catalog/MODIS\\_006\\_MCD64A1](https://developers.google.com/earth-engine/datasets/catalog/MODIS_006_MCD64A1)); MODIS MOD15A2H LAI data (<https://lpdaac.usgs.gov/products/mod15a2hv006/>); MODIS MCD43A3 albedo data ([https://developers.google.com/earth-engine/datasets/catalog/MODIS\\_006\\_MCD43A3](https://developers.google.com/earth-engine/datasets/catalog/MODIS_006_MCD43A3)); MODIS MOD16A2 ET data ([https://developers.google.com/earth-engine/datasets/catalog/MODIS\\_006\\_MOD16A2](https://developers.google.com/earth-engine/datasets/catalog/MODIS_006_MOD16A2)); CMRSET ET data ([https://developers.google.com/earth-engine/datasets/catalog/TERN\\_AET\\_CMRSET\\_LANDSAT\\_V2\\_2](https://developers.google.com/earth-engine/datasets/catalog/TERN_AET_CMRSET_LANDSAT_V2_2)).

## Acknowledgments

This study was supported by the National Key R&D Program of China (Grant 2022YFC3002804), the National Natural Science Foundation of China (Grant 41971032), the CAS Pioneer Talents Program, the CAS-CSIRO drought propagation collaboration project, and the CAS International Partnership Program (Grant 183311KYSB20200015). We appreciate the Editor Charles H. Luce, the anonymous Associate Editor and five anonymous referees for their constructive and critical comments that greatly improved the quality of the manuscript. We thank the Queensland Department of Environment and Resource Management for providing climate data, the Australian Bureau of Meteorology for providing streamflow data, the OzFlux and the FLUXNET community for providing flux tower data, the GRACE JPL team for providing terrestrial water storage anomaly data, and the MODIS team for providing the Collection 6 of burned area, LAI and albedo data. We also like to thank the Google Earth Engine platform for accessing these remote sensing data.

## References

- Abram, N. J., Henley, B. J., Sen Gupta, A., Lippmann, T. J. R., Clarke, H., Dowdy, A. J., et al. (2021). Connections of climate change and variability to large and extreme forest fires in southeast Australia. *Communications Earth & Environment*, 2(1), 8. <https://doi.org/10.1038/s43247-020-00065-8>
- Atchley, A. L., Kinoshita, A. M., Lopez, S. R., Trader, L., & Middleton, R. (2018). Simulating surface and subsurface water balance changes due to burn severity. *Vadose Zone Journal*, 17(1), 180099. <https://doi.org/10.2136/vzj2018.05.0099>
- Bart, R., & Hope, A. (2010). Streamflow response to fire in large catchments of a Mediterranean-climate region using paired-catchment experiments. *Journal of Hydrology*, 388(3–4), 370–378. <https://doi.org/10.1016/j.jhydrol.2010.05.016>
- Bart, R. R., & Tague, C. L. (2017). The impact of wildfire on baseflow recession rates in California. *Hydrological Processes*, 31(8), 1662–1673. <https://doi.org/10.1002/hyp.11141>
- Beaudouin, H., & Rodell, M. (2020). *GLDAS Noah Land Surface Model L4 3 hourly 0.25 x 0.25 degree V2.1*. Goddard Earth Sciences Data and Information Services Center (GES DISC). <https://doi.org/10.5067/E7TYRXPJKWOQ>
- Beringer, J., Hutley, L. B., McHugh, I., Arndt, S. K., Campbell, D., Cleugh, H. A., et al. (2016). An introduction to the Australian and New Zealand flux tower network—OzFlux. *Biogeosciences*, 13(21), 5895–5916. <https://doi.org/10.5194/bg-13-5895-2016>
- Bladon, K. D., Emelko, M. B., Silins, U., & Stone, M. (2014). Wildfire and the future of water supply. *Environmental Science and Technology*, 48(16), 8936–8943. <https://doi.org/10.1021/es500130g>
- Blount, K., Ruybal, C. J., Franz, K. J., & Hogue, T. S. (2019). Increased water yield and altered water partitioning follow wildfire in a forested catchment in the western United States. *Ecohydrology*, 13(1), e2170. <https://doi.org/10.1002/eco.2170>
- Boer, M. M., Resco De Dios, V., & Bradstock, R. A. (2020). Unprecedented burn area of Australian mega forest fires. *Nature Climate Change*, 10(3), 171–172. <https://doi.org/10.1038/s41558-020-0716-1>
- Boisrame, G. F. S., Thompson, S. E., Tague, C., & Stephens, S. L. (2019). Restoring a natural fire regime alters the water balance of a Sierra Nevada catchment. *Water Resources Research*, 55(7), 5751–5769. <https://doi.org/10.1029/2018wr024098>
- Bonan, G. B. (2008). Forests and climate change: Forcings, feedbacks, and the climate benefits of forests. *Science*, 320(5882), 1444–1449. <https://doi.org/10.1126/science.1155121>
- Bowd, E. J., Blair, D. P., & Lindenmayer, D. B. (2021). Prior disturbance legacy effects on plant recovery post-high-severity wildfire. *Ecosphere*, 12(5), e03480. <https://doi.org/10.1002/ecs2.3480>
- Bren, L. J., & Lane, P. N. J. (2014). Optimal development of calibration equations for paired catchment projects. *Journal of Hydrology*, 519, 720–731. <https://doi.org/10.1016/j.jhydrol.2014.07.059>
- Brey, S. J., Barnes, E. A., Pierce, J. R., Swann, A. L. S., & Fischer, E. V. (2021). Past variance and future projections of the environmental conditions driving Western US summertime wildfire burn area. *Earth's Future*, 9(2), e2020EF001645. <https://doi.org/10.1029/2020ef001645>
- Brookhouse, M. T., Farquhar, G. D., & Roderick, M. L. (2013). The impact of bushfires on water yield from south-east Australia's ash forests. *Water Resources Research*, 49(7), 4493–4505. <https://doi.org/10.1029/wrcr.20351>
- Brown, A. E., Zhang, L., McMahon, T. A., Western, A. W., & Vertessy, R. A. (2005). A review of paired catchment studies for determining changes in water yield resulting from alterations in vegetation. *Journal of Hydrology*, 310(1–4), 28–61. <https://doi.org/10.1016/j.jhydrol.2004.12.010>







- Watkins, M. M., Wiese, D. N., Yuan, D.-N., Boening, C., & Landerer, F. W. (2015). Improved methods for observing Earth's time variable mass distribution with GRACE using spherical cap mascons. *Journal of Geophysical Research: Solid Earth*, 120(4), 2648–2671. <https://doi.org/10.1002/2014jb011547>
- Watson, F., Vertessy, R., McMahon, T., Rhodes, B., & Watson, I. (2001). Improved methods to assess water yield changes from paired-catchment studies: Application to the Maroondah catchments. *Forest Ecology and Management*, 143(1–3), 189–204. [https://doi.org/10.1016/S0378-1127\(00\)00517-X](https://doi.org/10.1016/S0378-1127(00)00517-X)
- Wiese, D. N., Landerer, F. W., & Watkins, M. M. (2016). Quantifying and reducing leakage errors in the JPL RL05M GRACE mascon solution. *Water Resources Research*, 52(9), 7490–7502. <https://doi.org/10.1002/2016wr019344>
- Wiese, D. N., Yuan, D.-N., Boening, C., Landerer, F. W., & Watkins, M. M. (2018). *JPL GRACE Mascon ocean, ice, and hydrology equivalent water height release 06 coastal resolution improvement (CRI) filtered version 1.0. Ver. 1.0*. PO.DAAC. <https://doi.org/10.5067/TEMSC-3MJC6>
- Wine, M. L., Cadol, D., & Makhnin, O. (2018). In ecoregions across Western USA streamflow increases during post-wildfire recovery. *Environmental Research Letters*, 13(1), 014010. <https://doi.org/10.1088/1748-9326/aa9c5a>
- Wine, M. L., Makhnin, O., & Cadol, D. (2018). Nonlinear long-term large watershed hydrologic response to wildfire and climatic dynamics locally increases water yields. *Earth's Future*, 6(7), 997–1006. <https://doi.org/10.1029/2018ef000930>
- Wutzler, T., Lucas-Moffat, A., Migliavacca, M., Knauer, J., Sickel, K., Šigut, L., et al. (2018). Basic and extensible post-processing of eddy covariance flux data with REddyProc. *Biogeosciences*, 15(16), 5015–5030. <https://doi.org/10.5194/bg-15-5015-2018>
- Zeng, Z., Wang, D., Yang, L., Wu, J., Ziegler, A. D., Liu, M., et al. (2021). Deforestation-induced warming over tropical mountain regions regulated by elevation. *Nature Geoscience*, 14(1), 23–29. <https://doi.org/10.1038/s41561-020-00666-0>
- Zhang, Y., Kong, D., Gan, R., Chiew, F. H. S., McVicar, T. R., Zhang, Q., & Yang, Y. (2019). Coupled estimation of 500 m and 8-day resolution global evapotranspiration and gross primary production in 2002–2017. *Remote Sensing of Environment*, 222, 165–182. <https://doi.org/10.1016/j.rse.2018.12.031>
- Zhang, Y., Peña-Arancibia, J. L., McVicar, T. R., Chiew, F. H. S., Vaze, J., Liu, C., et al. (2016). Multi-decadal trends in global terrestrial evapotranspiration and its components. *Scientific Reports*, 6(1), 19124. <https://doi.org/10.1038/srep19124>
- Zhang, Y., & Post, D. (2018). How good are hydrological models for gap-filling streamflow data? *Hydrology and Earth System Sciences*, 22(8), 4593–4604. <https://doi.org/10.5194/hess-22-4593-2018>
- Zhao, F., Xu, Z., & Zhang, L. (2012). Changes in streamflow regime following vegetation changes from paired catchments. *Hydrological Processes*, 26(10), 1561–1573. <https://doi.org/10.1002/hyp.8266>
- Zhou, Y., Zhang, Y., Vaze, J., Lane, P., & Xu, S. (2015). Impact of bushfire and climate variability on streamflow from forested catchments in southeast Australia. *Hydrological Sciences Journal*, 60(7–8), 1340–1360. <https://doi.org/10.1080/0262667.2014.961923>